International Journal of Greenhouse Gas Control 136 (2024) 104199

Contents lists available at ScienceDirect

International Journal of Greenhouse Gas Control

journal homepage: www.elsevier.com/locate/ijggc

Assessing the impact of sedimentary heterogeneity on CO_2 injection in fluvial meander-belt successions using geostatistical modelling informed by geological analogues

Jose M. Montero [a,*], Luca Colombera [b,*], Enrique Yuste [c], Na Yan [a], Nigel P. Mountney [a]

[a] Fluvial, Eolian & Shallow-Marine Research Group, School of Earth and Environment, University of Leeds, Leeds LS2 9JT, UK
[b] Dipartimento di Scienze della Terra e dell'Ambiente, Università di Pavia, Via Ferrata 1, Pavia 27100, Italy
[c] TotalEnergies, Abu Dhabi, United Arab Emirates

ARTICLE INFO

Keywords:
Meandering fluvial system
Facies modelling
Multi-point statistics
Dynamic simulation
Carbon capture
CCS

ABSTRACT

To optimize programmes of carbon capture and storage, it is crucial to understand how subsurface heterogeneity may control CO_2 dispersal in sedimentary reservoir successions. It is therefore necessary to evaluate the impact of subsurface modelling techniques on predictions in lithological and petrophysical heterogeneity, and on resulting dynamic behaviours. In this study, alternative idealized, unconditional static models were created that incorporate different types of sedimentary heterogeneities typical of fluvial meander-belt sedimentary successions, at different scales. These static models were produced using two different geostatistical algorithms based on multipoint statistics: SNESIM and DEESSE. Two alternative sets of geocellular grids were created that capture (i) macroscale levels of heterogeneity only (architectural elements) and (ii) both macro- and mesoscale (point-bar lithologies) heterogeneities, respectively. The geocellular models were populated with petrophysical data from a selected geological analogue (Barracouta Formation, Australia), imposing a depth-related trend based on the analysis of literature data. Porosity and permeability models were obtained via Gaussian random function simulations. These static models were used to simulate subsurface CO_2 injection over a 30-year period to enable tracking of plume propagation and a comparison between models incorporating different levels of facies heterogeneity. The study highlights the influence of the underlying facies framework on CO_2 dynamic simulations, since aspects of reservoir pressure redistribution and caprock pressure relief only emerge from models incorporating mesoscale features. Furthermore, predicted CO_2 plume displacement, injection rates and cumulative injected volumes are also affected by the facies-modelling approach. Modelling categories and strategies must be carefully selected in subsurface modelling workflows applied to plan CCS projects.

1. Introduction

In the coming decades, subsurface Carbon Capture and Sequestration (CCS) projects are expected to serve as a major solution to mitigate the effects of global warming (Global CCS Institute, 2020; Ringrose et al., 2021). CCS projects are increasingly recognized by the international community as a solution for controlling the concentration of anthropogenic carbon dioxide (CO_2) in the atmosphere. Currently, the majority of CO_2 emissions come from fossil fuel combustion (Nalley and LaRose, 2021). The burning of fossil fuels is estimated to account for 73% of total greenhouse gas emissions and for 92% of total anthropogenic CO_2 emissions in the USA. Approximately 170 million tonnes of oil equivalent (Mtoe) of energy were used in the UK in 2020, with the majority of this (78%) coming from fossil fuels for heating and electricity production (UK Office for National Statistics, 2022). As part of the Paris Agreement (UNFCCC, 2018), 194 countries pledged to implement new low-carbon technologies, and Carbon Capture and Storage (CCS) was cited as a possible mitigation pathway. Although many CCS projects are already operational (e.g., Big Sky in Montana, USA; Sleipner, offshore Norway; Southwest Hub project, Australia), there exists uncertainty with respect to the safety, efficiency and commercial viability of large-scale CCS ventures. Thus, the construction of geologically sound reservoir models will play a significant role in the development and management of CCS projects. For a CCS project to be successful, a subsurface carbon repository should provide: (i) sufficient storage volume; (ii) the capability to sustain operational injection rates; (iii) the ability to

* Corresponding authors.
E-mail addresses: josemiguelsyc@gmail.com (J.M. Montero), luca.colombera@unipv.it (L. Colombera).

https://doi.org/10.1016/j.ijggc.2024.104199
Received 17 April 2024; Received in revised form 4 July 2024; Accepted 11 July 2024
Available online 19 July 2024

host and confine CO_2 safely, without leakage and preserving wellbore stability (Espinoza and Santamarina, 2017); and (iv) the capacity to undergo injection at a depth where the CO_2 can exist as a supercritical fluid (Ambrose et al., 2008). Several mechanisms act to trap CO_2 in the subsurface: (i) structural or stratigraphic trapping in the reservoir rock (Iglauer, 2018); (ii) solubility trapping of CO_2 that becomes dissolved in the reservoir brine (Riaz and Cinar, 2014); (iii) capillary residual trapping of CO_2 in pore spaces (Gershenzon et al., 2017), and (iv) mineralization due to chemical reactions of CO_2 with minerals in the reservoir rock (Al-Khdheeawi et al., 2017).

In depleted hydrocarbon reservoirs, oil and gas extraction leaves behind a permeable and porous volume that can potentially be filled with CO_2. The original presence of hydrocarbons over geological timescales proves the suitability of the reservoir volumes for long-term CO_2 storage (Spiteri et al., 2005; Bennion and Bachu, 2008). Yet, predictions of the ultimate fate of the injected CO_2 and planning of the injection process require accurate understanding of geological heterogeneity. Thus, skills and practices associated with the investigation of conventional hydrocarbon reservoirs, and reservoir modelling in particular, play a significant role in the prediction of volumetrics, injection rates, seal integrity, and injected-plume behaviour (Bachu et al., 2007; Budinis et al., 2018).

Sedimentary heterogeneity acts as a primary control on the distribution and mobility of resources in subsurface sedimentary successions. Hence, reservoir models incorporating lithological heterogeneities are routinely used to predict how fluids will move through subsurface reservoir volumes (Walker, 1984; Hickin, 1993; North, 1996; Brandsæter et al., 2001). Lithological heterogeneity has also been shown to exert a fundamental control on the performance of CO_2 sequestration plays (Reading, 2001; Lunt et al., 2004; Ringrose and Bentley, 2015). Static reservoir models incorporate structural geological features and sedimentary architectures and heterogeneities (henceforth *facies*). Commonly, geologically unrealistic facies models are a root cause for discrepancies between volumetric analysis and production forecasting against actual production results (i.e., history-matching discrepancies) (Caers and Zhang, 2004). Robust facies models, built using appropriate modelling algorithms and incorporating relevant sedimentary architectures and heterogeneities, are important for obtaining realistic predictions of the behaviour of a CO_2 plume in the subsurface (Flett et al., 2007; Singh et al., 2010; Eiken et al., 2011; Dai et al., 2014; Stalker et al., 2014; Soltanian et al., 2016; Nguyen et al., 2017). Special attention should be given to issues of stratigraphic compartmentalization, which may impede the lateral propagation of injected CO_2, and to facies-related heterogeneity in petrophysical properties and relative permeability curves, which impact CO_2 plume dynamics (Flett et al., 2007; Spiteri et al., 2005; Juanes et al., 2006; Nguyen et al., 2017).

A class of sedimentary successions that is of interest for CCS projects and that is noticeable for the presence of significant heterogeneities at multiple scales is the stratigraphic record of meandering fluvial systems (Cabello et al. 2018; Sun et al. 2023). The morphodynamics of meandering rivers results in the deposition and preservation of a complex arrangement of geo-bodies of variable geometry and lithological make-up (Miall, 1985, 1988, 2016; Bridge, 2003; Gibling, 2006). The spatial distribution, internal heterogeneity and connectivity of channel fills, barform elements and related overbank (e.g., levee, crevasse-splay) elements is highly variable and difficult to predict. In meander-belt successions, two broad categories of heterogeneity expressed at different scales can be identified: in this study, these are termed ‘macroscale’ and ‘mesoscale’ levels (cf. Friend 1983; Tyler and Finley 1991; Riordan et al. 2004; Colombera et al., 2013; Issautier et al. 2013). Macroscale heterogeneity pertains to the architectural products of deposition in specific meander-belt sub-environments, that is, they represent facies associations expressed as architectural elements (cf. Miall 1985; Colombera et al. 2013). At this scale, static reservoir models seek to represent the arrangement of sandbodies (e.g., point-bar elements) embedded in or juxtaposed with relatively fine-grained deposits (e.g., floodplain deposits, channel-abandonment mud plugs) (Fig. 1). The term mesoscale refers to smaller-scale lithological variability observable inside macroscale architectural elements: this might be expressed as beds and bedsets, commonly arranged in a predictable manner within their parent architectural elements (e.g., stratal packages defining fining-upward trends in a point-bar element). Smaller-scale heterogeneities at sub-bed scale are also present but are not considered in this study. It has been shown that representation of both macroscale and mesoscale heterogeneities in 3D reservoir models determines the ability of dynamic simulations to effectively map and predict fluid recovery or injection efficiency and storability (Cabello et al., 2018; Puig et al., 2019; Willis and Sech, 2019a, 2019b).

From a practical standpoint, however, producing static reservoir models for the successions of meandering fluvial systems that incorporate both macro- and mesoscale heterogeneities is not straightforward, due to the geometric, lithological and topological complexity of these heterogeneities. A major challenge is to design workflows that enable such elements to be incorporated effectively in 3D geocellular models while honouring conditioning data (i.e., hard data, such as borehole observations, and soft data, such as geophysical attributes). Traditionally, a variety of geostatistical methods have been used to model stratigraphic architectures. Yet, common methods based on two-point statistics (variograms) are largely ineffective at producing geologically realistic outputs (Pyrcz and Deutsch, 2014). Object-based methods are able to generate geometrically sensible representations of geobodies, but commonly suffer from convergence issues with large conditioning datasets (Haldorsen and MacDonald, 1987; Holden et al., 1988; Larue and Hovadik, 2006). Rule-based methods have shown promise as a way to produce geologically sound models, but are only applicable in special cases where meander-belt accretion geometries can be mapped or reconstructed in some detail (Colombera et al., 2018).

By contrast, modelling approaches based on multipoint statistics (MPS) use idealized geological models as training images to integrate geological information into reservoir models. This class of models combines the ability to fully honour well data with the capability to reproduce complex geometries and spatial relationships (Guardiano and Srivastava, 1993; Strebelle, 2002; Liu et al., 2004). These advantages make MPS methods well-suited for modelling fluvial meander-belt successions (Montero et al., 2021).

1.1. Aim and objectives

This research seeks to understand how scales of sedimentary heterogeneity considered in facies models for fluvial meander-belt sedimentary successions may impact CO_2 plume injection in a CCS reservoir volume. The specific objectives of this study are as follows: (i) to assess how the scale of focus at which sedimentary heterogeneities are reproduced in facies models (macroscale vs mesoscale) affects dynamic simulations of CO_2 injection over decadal timescales; and (ii) to evaluate the impact of the choice of geostatistical facies-modelling algorithm (‘single normal equation simulations’ vs ‘direct sampling’) on static model outputs and resulting dynamic behaviour, relative to the impact of the heterogeneity modelling scale.

2. Methodology

The workflow followed in this study includes the following steps: (i) unconditional geostatistical facies modelling of successions of fluvial meandering systems using MPS methods; (ii) construction of property models of porosity and permeability constrained by the facies models and informed by geological analogues; and (iii) dynamic simulations of CO_2 plume injection in the property models (Fig. 2).

2.1. Facies modelling

In meandering river systems, point-bar elements form due to

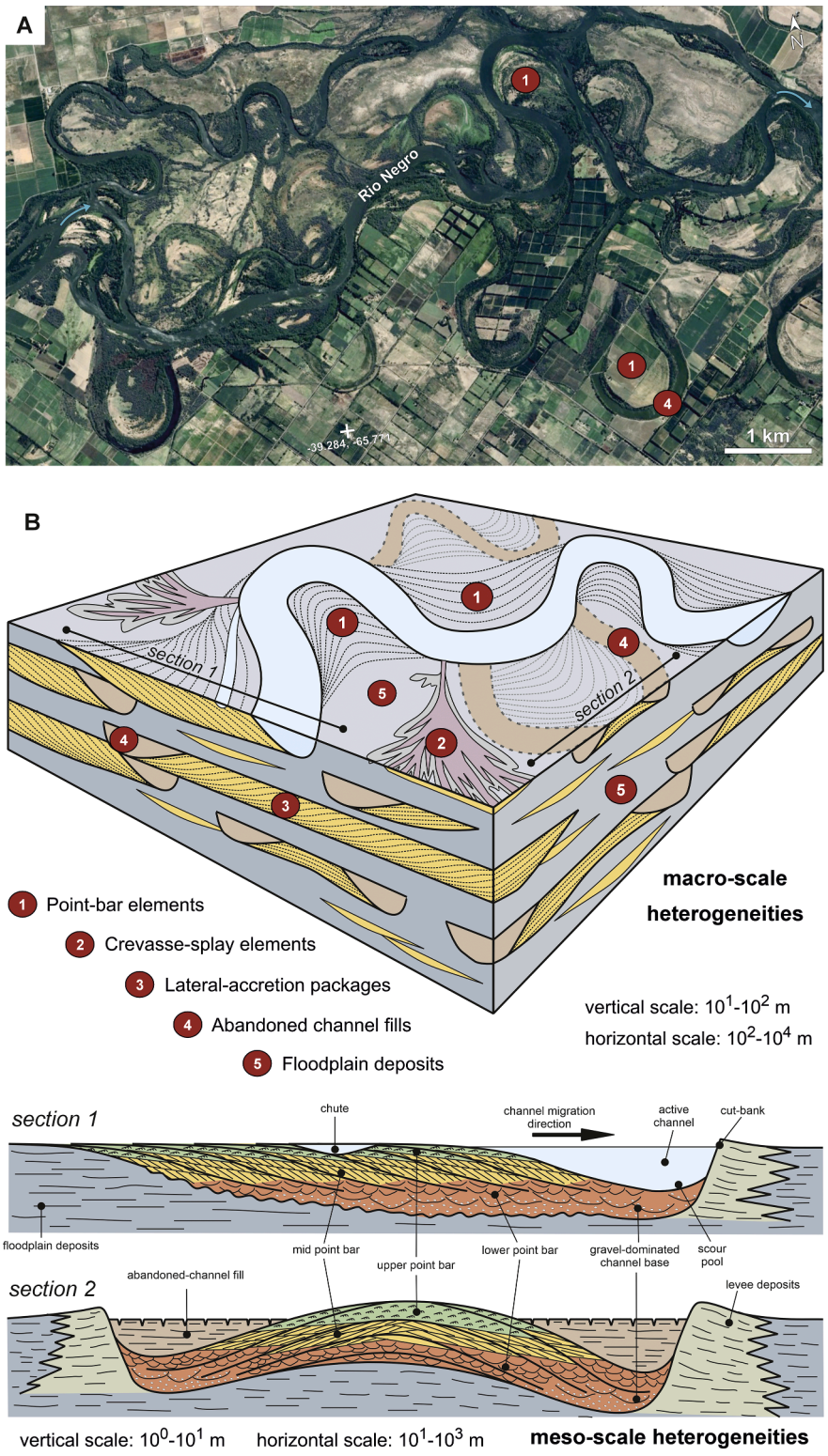

Fig. 1. A) Satellite image of a reach of the Rio Negro channel belt, Argentina, exhibiting the typical planform architecture of meander-belt sedimentary units. B) Block diagram and associated cross-sections of a sedimentary succession of a meandering fluvial system showing both macro- and mesoscale heterogeneities (Modified after: Ghazi and Mountney, 2009; Shiers et al., 2014). Ranges of typical vertical and horizontal scales are indicated.

meander-bend migration and concurrent deposition on the inner bank of a channel, until that channel is eventually abandoned following bend cut-off or avulsion. The abandoned channel can then be infilled by sediment transported in suspension by floods. Meander belts typically consist of mosaics formed by multiple preserved point-bar elements bordered by channel-fill deposits: these elements are the macroscale features of interest in this study (Fig. 1). Internally, these features may exhibit smaller-scale heterogeneities: these are the mesoscale entities considered here (Fig. 1).

This study applied a workflow for modelling meander-belt successions based on MPS modelling algorithms; the workflow and its outputs are discussed in detail by Montero et al. (2021) (Fig. 2). In the workflow,

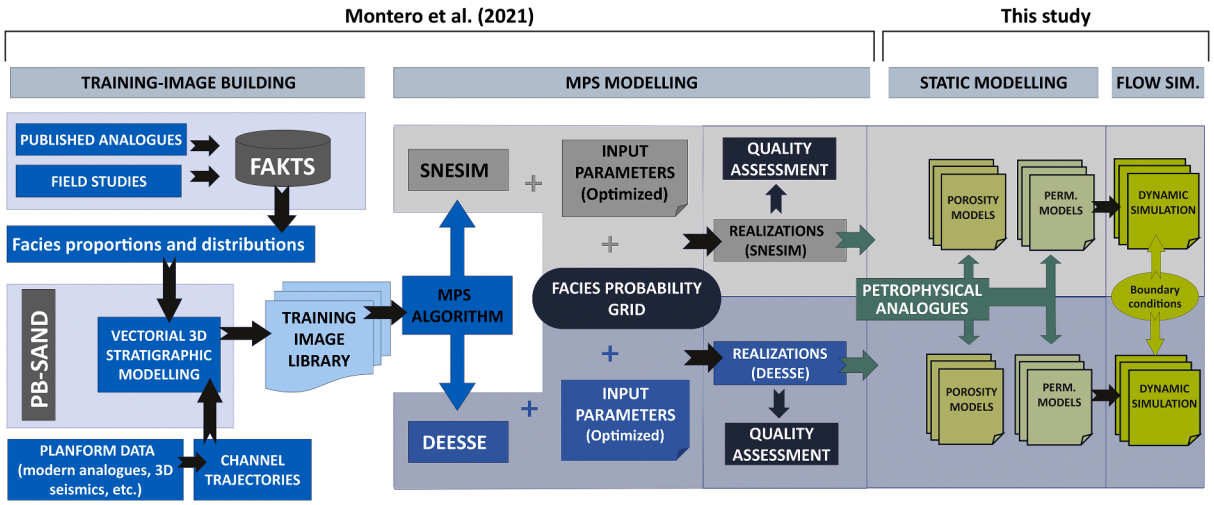

Fig. 2. Workflow for static modelling and dynamic simulation followed in this study. See text for explanation.

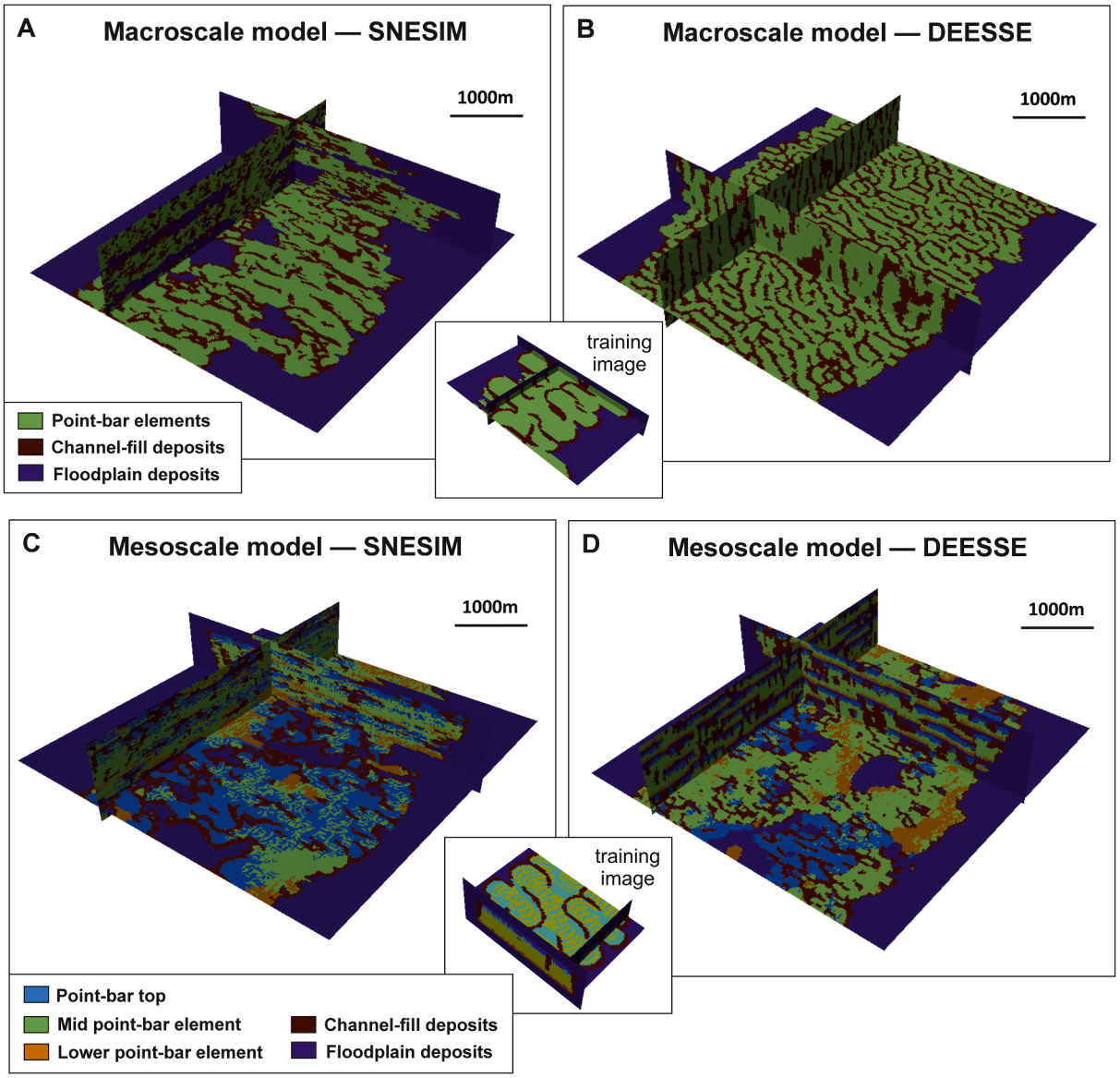

Fig. 3. Four realizations obtained from SNESIM (A, C) and DEESSE (B, D) using training images for macroscale (A, B) and mesoscale (C, D) features. Vertical exaggeration set to a factor of 25.

MPS training images were created using a forward stratigraphic modelling software (Point-Bar Sedimentary Architecture Numerical Deduction, PB-SAND; Yan et al., 2017) that simulates fluvial meander-bend evolution and resulting point-bar facies organization. PB-SAND model inputs were defined based on data from multiple geological analogues included in a relational database which stores sedimentological data from many fluvial sedimentary successions (the Fluvial Architecture Knowledge Transfer System, FAKTS; Colombera et al., 2012a, 2012b, 2013, 2017). The training images that were derived this way were applied to two different MPS algorithms: SNESIM (Single Normal Equation SIMulation; Strebelle, 2002), and DEESSE (Direct Sampling; Mariethoz et al., 2010). A key difference between the two approaches is that in the case of SNESIM spatial patterns are saved in a search-tree database, whereas in the case of DEESSE the patterns are extracted by directly scanning the training image. MPS modelling algorithms tend to produce spatially stationary outputs; yet auxiliary variables can be used to force incorporation of spatial trends (e.g., facies proportions, element orientations) in the models (cf. Montero et al. 2021).

A set of eighty facies realizations has been produced via MPS modelling, of which four are employed in the work presented here. These four realizations result from the combination of: (i) two training images, each incorporating different types of lithological heterogeneities, and (ii) the two modelling algorithms (SNESIM and DEESSE). The two training images, and their corresponding facies realizations, incorporate sets of three and five lithological ('facies') types, corresponding to macroscale and mesoscale heterogeneities, respectively. In facies models with macroscale focus, three rock types are included: (i) mudstone that was accumulated in floodplain areas; (ii) sandstone deposited in point-bar settings in the channel belt of a meandering river, of which the main reservoir units are made; and (iii) mud-prone channel-fill deposits that can act as baffles or barriers to the flow in the channel-belt deposits. In facies models with mesoscale focus, point-bar deposits are themselves differentiated into three different categories of point-bar lithologies (mesoscale heterogeneities): (i) coarser lower point-bar deposits that accumulated near the channel thalweg; (ii) sand-prone mid point-bar deposits; and (iii) finer-grained point-bar top deposits. These three categories are arranged according to a vertical fining-upward trend reproduced in the training images used to obtain the MPS realizations. At a larger scale, the stacking pattern of meander-belt deposits is representative of the infill of an alluvial valley (Montero et al., 2021).

The four selected facies realizations (Fig. 3) are used as frameworks for the creation of property (porosity and permeability) models, as explained below. Details on the inputs to the facies modelling algorithms are presented in Montero et al. (2021).

2.2. Selection of petrophysical data and property modelling

The idealized facies models used in this investigation were populated with representative petrophysical data derived from geological analogues (**Supplementary Material 1**). Data on porosity and permeability of sedimentary units from fluvial successions were compiled by drawing data from the scientific literature and technical reports; this dataset was collated to facilitate the creation of property models in data-poor contexts; a similar approach has been commonly adopted in compiling other analogous databases (e.g., P3 – Petrophysical Property Database, Bär et al., 2020; BritGeothermal database, British Geological Survey; National Geothermal Data System, United States Geological Survey). The dataset collated for this study is unique in that it brings together analogue data on petrophysical properties in a way that enables such properties to be linked directly to sedimentological characteristics. The collated dataset incorporates more than 4000 records of petrophysical parameters (mainly porosity and permeability) from 48 case studies (**Supplementary Material 1**), stored alongside additional attributes, such as sedimentary structures, petrographic composition, lithofacies type, architectural-element type, age of the deposit, formative palaeoenvironment, and associated metadata. The data are extracted from outcrop, core and well-log datasets of fluvial sedimentary deposits.

The petrophysical data included in the database were used in two ways: (i) to identify analogue datasets of petrophysical properties (porosity and permeability) relevant to fluvial successions targeted for CCS; a specific geological analogue was chosen in view of its match in terms of depositional context and geological architecture and its potential as a CCS target (see Section 2.2.1 below); (ii) to assess correlations and spatial trends for petrophysical properties of specified types of sedimentary units.

Property models for each of the four facies models described above were obtained by populating the 3D grids with petrophysical properties whose distributions are constrained by the modelled facies. Porosity and permeability models were created in Schlumberger Petrel™ using the Sequential Gaussian Random Function Simulation (GRFS) algorithm. In the GRFS algorithm, anisotropy in the property being simulated is controlled via variogram models with specified ranges. Arbitrary values of major, minor (both on the horizontal plane), and vertical variogram ranges were selected based on visual analysis of the size of point-bar features observed in the previously built facies models (Table 1). An exponential variogram model was used for all property models. The GRFS algorithm was also conditioned on trends that describe correlations between different properties (namely, between depth and porosity and between porosity and permeability) and spatial relationships (often expressed by vertical and lateral trends) between different modelling categories (facies). Equations obtained via regression were used as follows: (i) a depth-porosity transform for each facies type was used in the creation of porosity models; (ii) porosity-permeability transforms were applied to previously modelled 3D porosity volumes for each facies type in the creation of permeability models. No horizontal trends are incorporated in the simulations. The inputs to the porosity and permeability models are summarized in Table 1. The petrophysical trends were derived from the analysis of the analogue petrophysical dataset for the sedimentary units included in the facies models. A range of geological analogues was considered for deriving relevant data on petrophysical properties. Analogue-derived information employed in the property modelling and the grid configuration are summarized in Table 1. For both macro- and mesoscale property models, a single reservoir zone was modelled as a grid of 250 cells along both horizontal directions, and 50 cells along the vertical direction. The cell size was set at 20 m along both horizontal directions and 1 m vertically. The modelled gridded volume was treated as occurring over depths of 2,350–2,400 m.

2.2.1. The Latrobe Group

A specific geological analogue was used in this study for extracting petrophysical data with which to constrain the property models: the Late Cretaceous-Eocene Latrobe Group in the Gippsland Basin (SE Australia), as observed in cores of the Tarwhine-1 well (WAPIMS database - Western Australia Department of Mines, Industry Regulations and Safety). The Latrobe Group sandstone units are the primary reservoirs in the Gippsland Basin (Petroconsultants, 1996), but are also considered as potential targets for CCS programmes (Bunch et al., 2011; Langford, 2016). Thus, several projects are now investigating the suitability of this succession, and the Gippsland Basin more widely, for CCS (Quinn, 2022). The Tarwhine-1 well intersects the Barracouta Formation, which comprises a gas-prone reservoir (Moore et al., 1992) and includes reservoir units targeted for CCS. The Barracouta Formation is part of the Halibut Subgroup, which is Maastrichtian to early Eocene in age (ca. 75 to 45 Ma) and was accumulated in a rift-related extensional basin. Parts of the Barracouta Formation are interpreted as having been deposited in a meandering fluvial environment, whose preserved stratigraphy is characterized by significant sandbody compartmentalization. Fluvial reservoir sandstone bodies are commonly made of texturally mature and moderately well-sorted sandstone, with porosity values that are typically in the 15–25% range. The Barracouta Formation includes

Table 1
Summary of inputs to porosity and permeability models. Φ = porosity, z = depth, k = permeability.

	Porosity models			Permeability models		
	Model macroscale	Model mesoscale		Model macroscale	Model mesoscale	
	Point-bar elements	Lower bar elements	Upper bar elements	Point-bar elements	Lower bar elements	Upper bar elements
Method	Transform (co-kigring)	Transform (co-kigring)	Transform (co-kigring)	Transform + 3D volume porosity (co-kriging)	Transform + 3D volume porosity (co-kriging)	Transform + 3D volume porosity (co-kriging)
Porosity and permeability transform	Φ = 0.0039 + 21.001*z	Φ = 4305.58 − 147.83*z	Φ = 3374.61 − 111.09*z	Log10(k) = − 0.66 + 0.14*Φ	Log10(k) = 1.88 + 0.26*Φ	Log10(k) = 1.96 + 0.15*Φ
Minimum value	0.11	0.12	0.08	9 mD	29 mD	0.2 mD
Maximum value	0.12	0.14	0.1	10 mD	37 mD	0.33 mD
Mean value	0.117	0.1307	0.09	9.6 mD	32.82 mD	0.24 mD
Variogram range SNESIM (m)	200 × 200 × 5	300 × 300 × 5	300 × 300 × 5	200 × 200 × 5	300 × 300 × 5	300 × 300 × 5
Variogram range DEESSE (m)	250 × 250 × 5	250 × 250 × 5	250 × 250 × 5	250 × 250 × 5	250 × 250 × 5	250 × 250 × 5

high-quality sandstone, some of which displays multi-Darcy permeabilities. However, porosity and permeability values from observations made in the Tarwhine-1 well are in the lower end of the overall ranges for the formation. Secondary porosity due to dissolution of dolomite cement associated with hydrocarbon emplacement is the main porosity contributor in the Latrobe Group, whereas authigenic kaolinite growth, chlorite filling, quartz cementation and overgrowths occluded part of the original porosity (Bunch et al., 2011). Porosity-versus-depth plots indicate a severe decline in porosity with depth; this limits the reservoir viability beneath approximately 4,000 m depth (Clark and Thomas, 1988).

2.2.2. Porosity models

In facies models incorporating mesoscale heterogeneities, a constant effective porosity equal to zero was selected for floodplain and channel-fill deposits, so that corresponding cells would be deactivated in the dynamic simulations. Thus, floodplain and channel-fill deposits behave as non-permeable barriers in the macroscale facies models.

For point-bar deposits, a porosity-depth relationship was used to account for sediment compaction in the Latrobe Group; the derived function (transform) was applied for constraining the porosity realizations. In the petrophysical analogue dataset, different linear depth-porosity trends were observed corresponding to different compaction regimes: a relationship between porosity and depth applicable to the Latrobe Group was considered (Table 1), on the basis of the moderate compaction reported in the completion report for well Tarwhine-1. The trend was then applied to the simulations as a secondary variable in collocated co-kriging, on both SNESIM and DEESSE facies models. No horizontal trend was included. Fig. 4 shows two representative porosity realizations based on facies models produced with SNESIM and DEESSE.

A similar workflow was followed for the facies models with mesoscale focus. Porosity-depth trends to be used as secondary variables were chosen for each of the three point-bar lithological categories. Analogue data on the porosity of lower point-bar and point-bar top deposits yield the porosity-depth trends in Table 1. The Latrobe Group porosity values considered for point-bar deposits in the facies models for macroscale heterogeneity were applied to the middle point-bar facies type. Porosity realizations for the facies models with macroscale focus are shown in Fig. 4.

2.2.3. Permeability models

The approach taken to model permeability also includes the use of secondary data. For facies models with macroscale heterogeneities only, permeability modelling of point-bar strata was undertaken by (i) applying a porosity-permeability trend derived from analysis of the Latrobe Group (Table 1), and (ii) by using previously built porosity realizations to condition the permeability values (Fig. 4). Because of the narrow range in porosity values, the permeability field is characterized by effectively constant values across the point-bar domains. Although this scenario is not realistic from a geological standpoint, it allows the influence of the presence of effectively impermeable units acting as flow barriers to be examined. For facies models with mesoscale heterogeneities, three different porosity-permeability trends were used for lower point-bar, middle point-bar and point-bar top facies: two transforms were determined for lower and upper point-bar deposits (Table 1), whereas the porosity-permeability relationship used for point-bar deposits in the macroscale model was applied to the middle point-bar class. The previously built porosity models were also used to co-krige the simulations. This results in a permeability field that is more geologically realistic than the one obtained for macroscale models. In both sets of models, cells corresponding to floodplain and channel fill deposits were set arbitrarily as having a porosity equal to zero, so that they would become deactivated in the dynamic simulations; as such, no permeability value was required to be assigned to these cells. Inputs to the geostatistical modelling algorithm are reported in Table 1. Example permeability realizations are presented in Fig. 5.

2.3. Dynamic simulations

The grid resolution of the facies and property models (20 m horizontally, 1 m vertically) was maintained for the dynamic simulations, in view of the need to capture detailed facies and petrophysical heterogeneity. Dynamic simulations of CO_2 injection were run using the simulator Schlumberger Eclipse E300. The operational set-up includes a master injection well (INJ-1, located at X: 2250, Y: 2500), which is the main focus of the analyses, and a second injector well (INJ-2; X: 2250, Y: 3450), which acts as a comparison well for assessing the representativeness of the results. Both wells were completed over the entire depth interval of interest, from 2,350 m to 2,400 m.

A fluid model including gas and water was defined in the depleted gas field targeted by the Tarwhine-1 well at 2,350 m. The fluid-flow model corresponds to a standard pre-set of CO_2 gas and water. A constant water saturation of 0.98 (S_w) was considered such that the gas saturation constant (S_g) is equal to the complement of water saturation (S_g=1-S_w). The reservoir was then initialized as almost fully saturated with brine at the beginning of the simulations to replicate a gas reservoir that has been produced up to the gas critical saturation point (S_{gr}). Injected CO_2 and water solubility effects in the reservoir were considered in the simulations. CO_2 physical properties, including density, viscosity, solubility and supercritical behaviour, were defined based on experimental data that are typical for CO_2 storage conditions (12–250 °C and up to 600 bars; Haghbakhsh et al., 2013). No thermal exchange was considered in the simulations. Maximum reservoir pressures in the model were set to 442.27 bar, in agreement with a calculated fracture

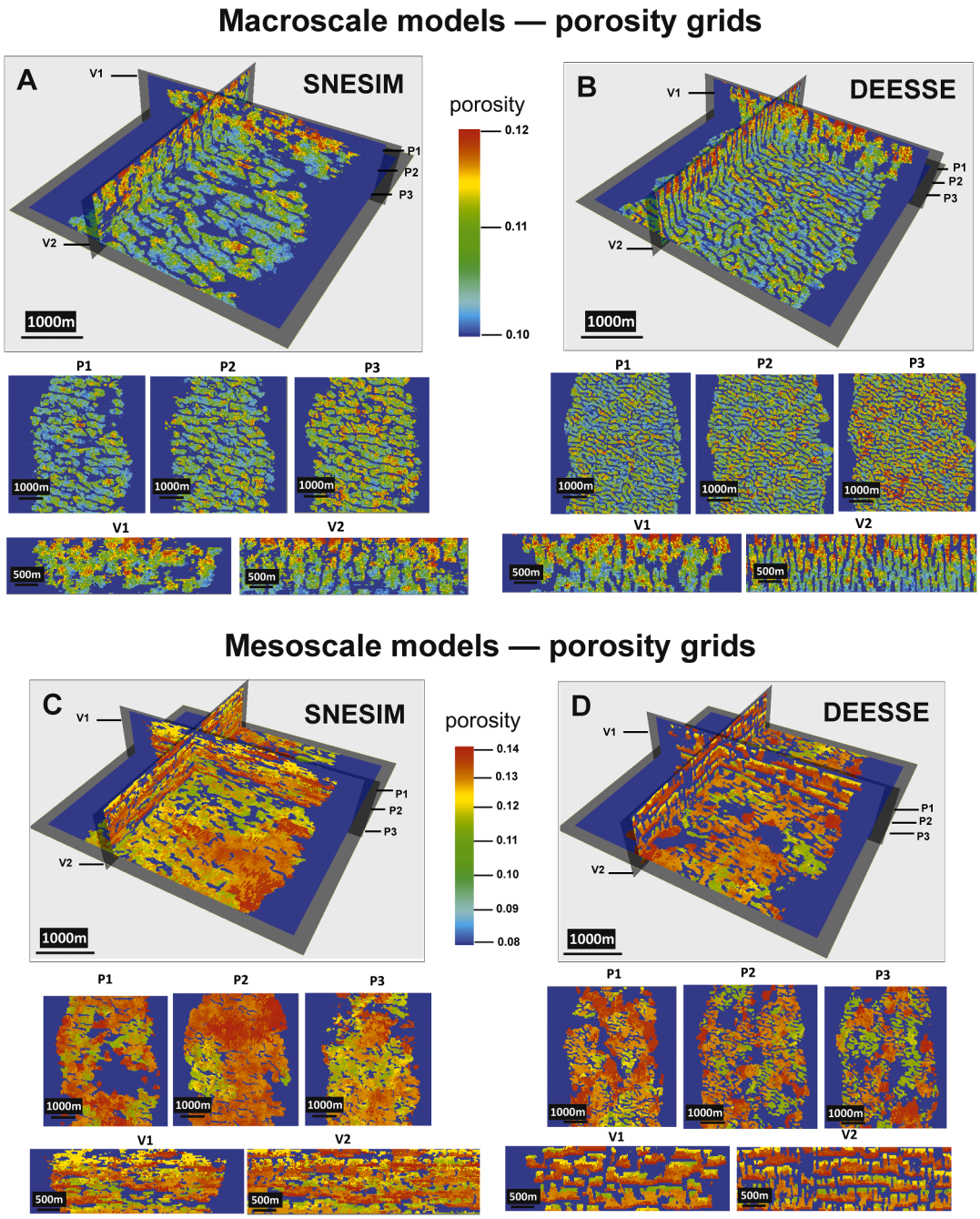

Fig. 4. Porosity models for corresponding facies models with macroscale (A, B) and mesoscale (C, D) focus, obtained via geostatistical modelling operated on SNESIM (A, C) and DEESSE (B, D) realizations. Vertical exaggeration set to a factor of 25.

gradient using sonic-log data as pressure indicator obtained from the WAPIMS database for well Tarwhine-1. The pore pressure at 2,350 m was set as 281.9 bar according to Eaton's method. A geothermal gradient of 55 °C/km was selected based on data from the Snapper field (Glenton, 1991), the closest offset field where an accurate geothermal gradient was calculated. This results in temperatures between 129 °C and 132 °C in the interval of investigation. A saline aquifer has been included that extends across the boundaries of the model.

The permeability and porosity models were used as inputs to the dynamic simulations. Permeability values in vertical and horizontal directions were considered to be equal. Relative permeabilities were considered in this study based on Corey's permeability curves (Corey, 1954) for each of the model elements (Fig. 6) and considering a compositional fluid model of gas and brine. Corey's relative permeability relationship, which was created to describe oil and gas flow in porous media, can effectively be applied to CO_2 and brine flow (Bennion and Bachu, 2006; Moodie et al., 2014). Hysteresis effects in relative permeability have not been considered in the simulations.

Using this approach, the residual water saturation (S_{wi}) and the critical gas saturation (S_{gr}) endpoints were calibrated for each of the lithological categories (facies). A standard compaction model for consolidated sandstones was established using a minimum pressure of 262.10 bar (hydrostatic gradient at 2,350 m) and a maximum pressure of 442.27 bar (fracture gradient at 2,350 m). Rock compressibility was set to 1.45×10^{-5} bar. The modelled porosity values were additionally used to control porosity-depth dependencies in the rock compressibility model. No adsorption or Leverett J-function for capillary pressure were taken into account in this study.

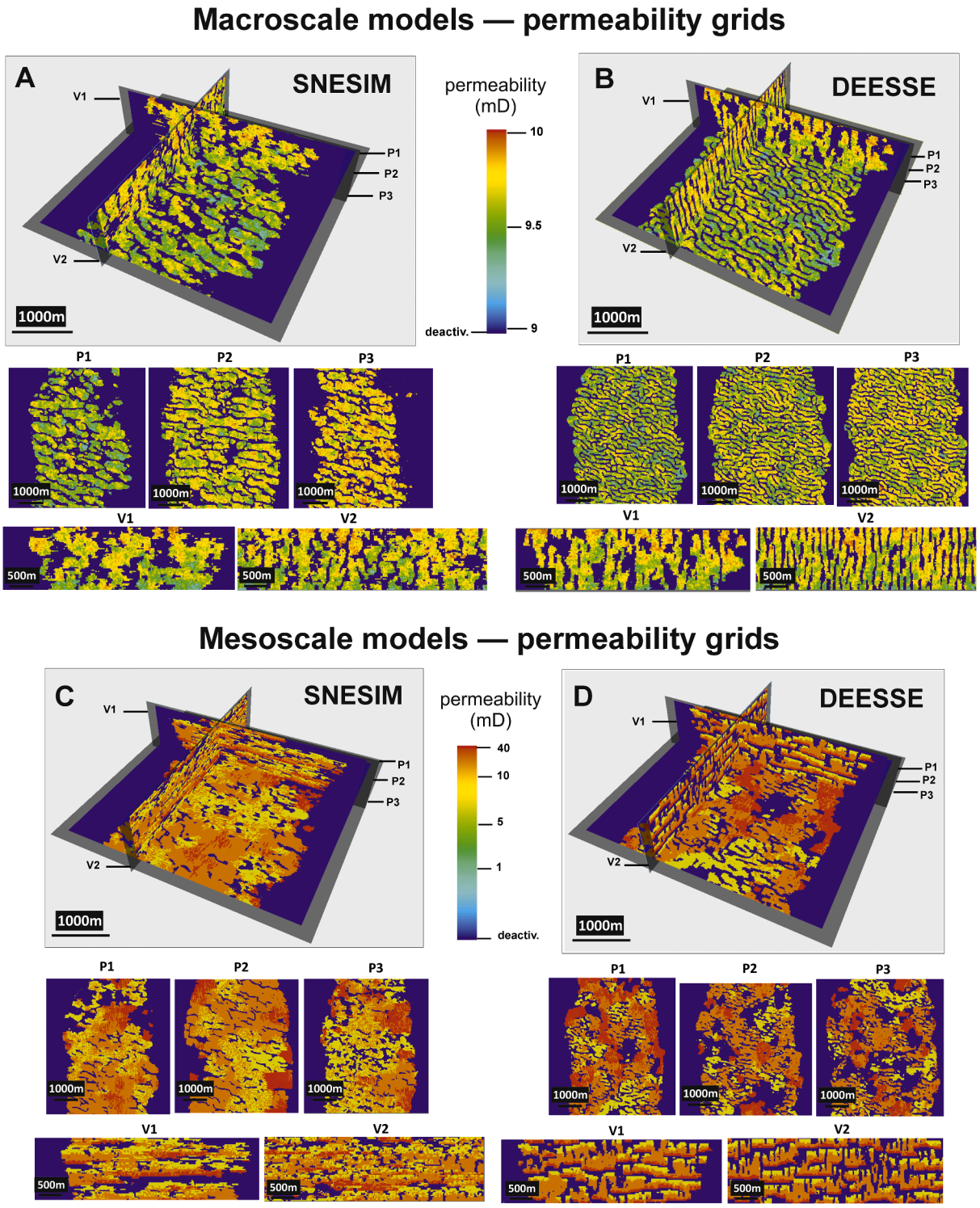

Fig. 5. Permeability models for corresponding facies models with macroscale (A, B) and mesoscale (C, D) focus, obtained via geostatistical modelling operated on SNESIM (A, C) and DEESSE (B, D) realizations. In the colour scale, blue domains labelled with 'deactiv.' refer to cells that were set as deactivated in the subsequent flow simulations. Vertical exaggeration set to a factor of 25.

A development plan was considered where CO_2 is injected at constant 430 bar bottom-hole pressure; it should be noted that this value is only marginally lower than the fracture pressure (442 bar), and so may not be compliant with CCS regulations globally. The simulation time length considers the average life span of a CO_2-emitting coal-fired power station, which is approximately 30 years. Therefore, three different time steps were evaluated for injection over 5, 10 and 30 years, for each of the realizations (SNESIM and DEESSE; macro- and mesoscale facies). Years five and ten were considered as intermediate steps for monitoring plume migration. Each grid consisted of a total of 3.125 million cells. Dynamic simulations were optimized so as to limit runtime to up to 4 h per 5 years of simulation time. To do so, all cells with permeability values below 0.1 mD were deactivated. This allows the dynamic simulations to run faster. The average runtime for the facies models with macroscale heterogeneities only was approximately 45 min per year of simulation, using a conventional personal computer with a 6-core CPU (AMD Ryzen 5 3,600

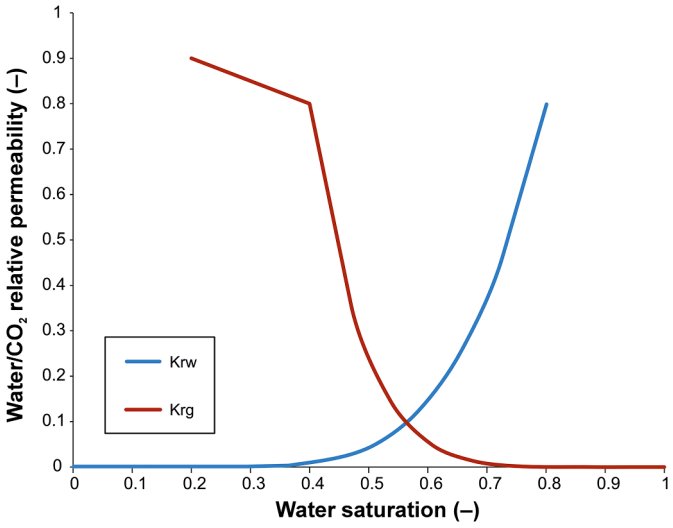

Fig. 6. Relative permeability curves defined for the point-bar elements of the macroscale models and the mid-point-bar deposits of the mesoscale models.

MHz) and 16 GB RAM. The average runtime for facies models including mesoscale heterogeneities was approximately twice as long.

3. Results

Results are presented separately for simulations run on macro- and mesoscale static models. Qualitative visual analyses are undertaken in this study with consideration of simulated pressure distribution, storage and injection rates.

3.1. Dynamic behaviour of macroscale models

Dynamic simulations of models incorporating macroscale heterogeneity only (sand-prone point-bar deposits with extremely limited petrophysical heterogeneity, and mud-prone channel-fill and floodplain deposits treated as effectively impermeable), produced with both SNESIM and DEESSE, portray a rapid spread of the injected CO_2 over the initial five years of injection (Fig. 7). Yet, brine displacement initiating from the original well location appears as discontinuous and non-linear through time. The CO_2 plume front does not spread homogeneously as it progresses in the grid; instead, the plume expands in a tortuous manner due to the presence of low-permeability obstacles incorporated in the MPS models and representing abandoned channel-fill deposits (mud plugs) or remnants of floodplain deposits, both of which may act as intra-channel-belt baffles to flow. However, differences in dynamic behaviour are seen, in relation to how mud-plug features vary in geometry across outputs from SNESIM and DEESSE. In simulations run on the DEESSE static model, the CO_2 plume takes a slightly more digitate planform morphology and more pronounced spatial variability in migration rates along the vertical column. The presence of mud-prone intraformational barriers at different elevations in the modelled valley fill impacts CO_2 storage by facilitating pressure relief on the overburden seal (Fig. 8).

From year 5 to year 30, preferential CO_2 flow pathways emerge, following an ENE-WSW direction in both SNESIM and DEESSE models. Along these pathways, the plume spreads at a faster horizontal rate than in the previous earlier stage. This is due to the presence of laterally connected sand-prone point-bar deposits, and therefore reflects the limited ability of the MPS modelling algorithm to reproduce laterally continuous mud plugs with loop-like planform shapes. In vertical sections it can be observed that the migration of CO_2 results in a funnel-shaped plume in realizations created with both SNESIM and DEESSE; however, vertical variability in plume propagation remains higher in the DEESSE realization. Although CO_2 saturation and pressures are slightly higher at shallower depths during the 30 years of injection, alarmingly high values of pressure or CO_2 saturation near the caprock are not attained. After 15 years, brine displacement occurs at a slower rate compared to the first stages of injection, as the surface area of the plume increases in size (Fig. 8).

3.2. Dynamic behaviour of mesoscale models

In dynamic simulations run on static models that incorporate mesoscale heterogeneities, the early stages of injection (initial five years) are again characterized by CO_2 flow that is mainly controlled by the presence of flow barriers (channel-fill and floodplain deposits) in the proximity of the wells, and by the connectivity and geometry of sand-prone facies. Once more, the plume propagates more rapidly in wider and thicker sand-prone conduits; however, the finer-scale petrophysical heterogeneity related to point-bar fining-upward trends becomes important in this case. Notably, the development of preferential pathways is more prominent in the simulation run on the SNESIM static model (Fig. 9). This reflects the relatively larger lateral continuity of higher-permeability lower and middle point-bar deposits in the SNESIM realization compared to the one obtained with DEESSE.

Compared to the results of dynamic simulations run on the facies model with macroscale heterogeneities only, in simulations of mesoscale models the CO_2 plume exhibits more significant variability in both propagation rate and direction of migration of its front. This becomes particularly apparent in the evolution of the CO_2 plume from year 5 to year 30, as seen on horizontal sections of both the SNESIM and DEESSE models. In planview, a markedly asymmetric propagation of the plume front is evident in these cases, with CO_2 flow pathways dictated by the presence and connectivity of lower and middle point-bar facies acting as thief zones (Fig. 10). At the same time, the point-bar top facies experience low saturation values and behave as baffles that force the CO_2 front towards the flow conduits, enhancing the lateral fingering of the plume. In vertical sections, the effects of lithological heterogeneity on CO_2 flow and saturation are also related to differences in relative permeabilities that exist between lower and middle point-bar deposits. Together with the presence of intraformational seals (non-permeable channel-fill and overbank deposits), the considered petrophysical heterogeneity helps distribute the CO_2 column at different elevations in the stratigraphic volume, reducing the pressure on the top seal.

3.3. Pressure distribution

In terms of pressure distribution, reservoir pressure values in facies models with both macro- and mesoscale focus are seen to depend on the geological heterogeneity found in proximity of the well. An example of this behaviour can be seen in dynamic simulations of facies models with macroscale heterogeneities only (Fig. 11): the model created with SNESIM is characterized by higher injection pressure values compared to the one created with DEESSE. This is due to presence of thicker and more continuous flow barriers located closer to the area of influence of the well, which affect sand-body connectivity and CO_2 flow pathways. On the contrary, the DEESSE facies framework, having higher sandstone connectivity, is characterized by flow conduits that exert a more pronounced pressure relief. However, the opposite behaviour can be observed for SNESIM and DEESSE models created for facies architectures considering mesoscale heterogeneities (Fig. 11). The geological heterogeneity in the models also affects pressure dissipation through time. In the models created with both SNESIM and DEESSE, pressure values around the injector decrease progressively after the first years of injection following water displacement in the proximity of the well. However, in models created with DEESSE, pressure dissipation is more effective in the grid that only includes macroscale heterogeneity, whereas in models created with SNESIM reservoir pressure is more readily dissipated in the grid that also incorporates mesoscale features.

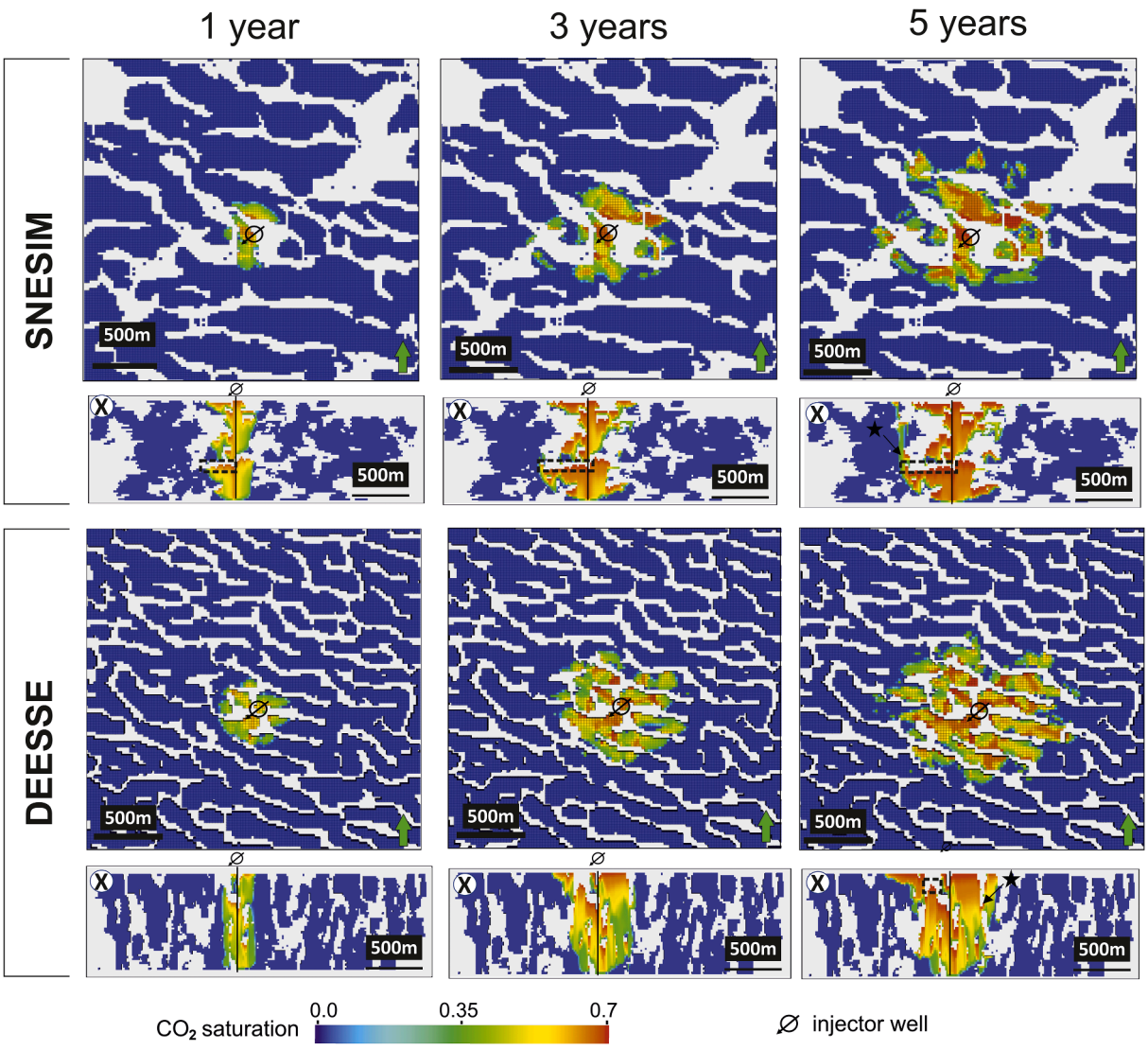

Fig. 7. Plume evolution on horizontal and vertical sections for macroscale-only facies models produced with SNESIM and DEESSE, for one, three and five years of injection. The blue colour indicates brine-saturated volumes. Barriers to flow are represented in white. Horizontal sections are extracted at $Z = 21$ (out of 50 slices). Black dashed frames highlight CO_2 accumulation under intraformational barriers. Black stars highlight interconnections between stratigraphic compartments. Vertical sections cross the location of the injector well INJ-1. Vertical exaggeration set to a factor of 25.

After 30 years of simulation, the majority of sand-prone reservoir volumes record a pressure effect due to injection, in facies models with both macro- and mesoscale focus. However, broad-scale reservoir pressurization is only seen taking place for SNESIM and DEESSE models that contain mesoscale heterogeneities, after 22 and 26 years, respectively. This pressurization event is not observed on simulations run on models that only include macroscale heterogeneities (Fig. 11).

3.4. Storage and injection rates

The dynamic behaviour of the different models has also been analysed in terms of storage capacity and injection rates. Results associated with injection at the primary injector well (INJ-1) have been complemented with those of dynamic simulations associated with the INJ-2 well, operated over 15 years. For the facies models with macroscale heterogeneity only, notable differences are observed for injection at INJ-1 and INJ-2, and across models built with different algorithms (Fig. 12). Cumulative CO_2 injected volumes are similar for SNESIM and DEESSE grids (Fig. 12A) when injection takes place at INJ-2; by contrast, cumulative volumes are different for the SNESIM and DEESSE grids when injection takes place at INJ-1, and these values are themselves different compared to INJ-2 results.

Discrepancies in storage capacity and injection rate between the four dynamic simulations reflect the effects of sedimentary architectures and associated petrophysical heterogeneity located in the surroundings of the injectors. The highest injection rates and injected volumes are seen for the simulation run on the DEESSE model with macroscale features only, with injection at well INJ-1. This well is drilled through well-connected sand-prone volumes with homogeneous petrophysical characteristics: these volumes provide efficient pathways along which the plume can migrate since the early injection stages. Temporal changes in injection rates can be identified in all simulations. The injection rate increases rapidly in the first few months due to bottom-hole pressure injection effects (430 bar), and subsequently declines in relation to near-wellbore pressure build-up. The dissolution of CO_2 into the brine hampers the formation of a distinct CO_2 phase in the reservoir, which has an impact on the relative permeability of CO_2. Afterwards, as the pore volume becomes saturated in CO_2, the formation of a distinct CO_2 phase leads to an increase in the injection rates. As CO_2 saturation increases, injection rates vary steadily through time because of the effect of

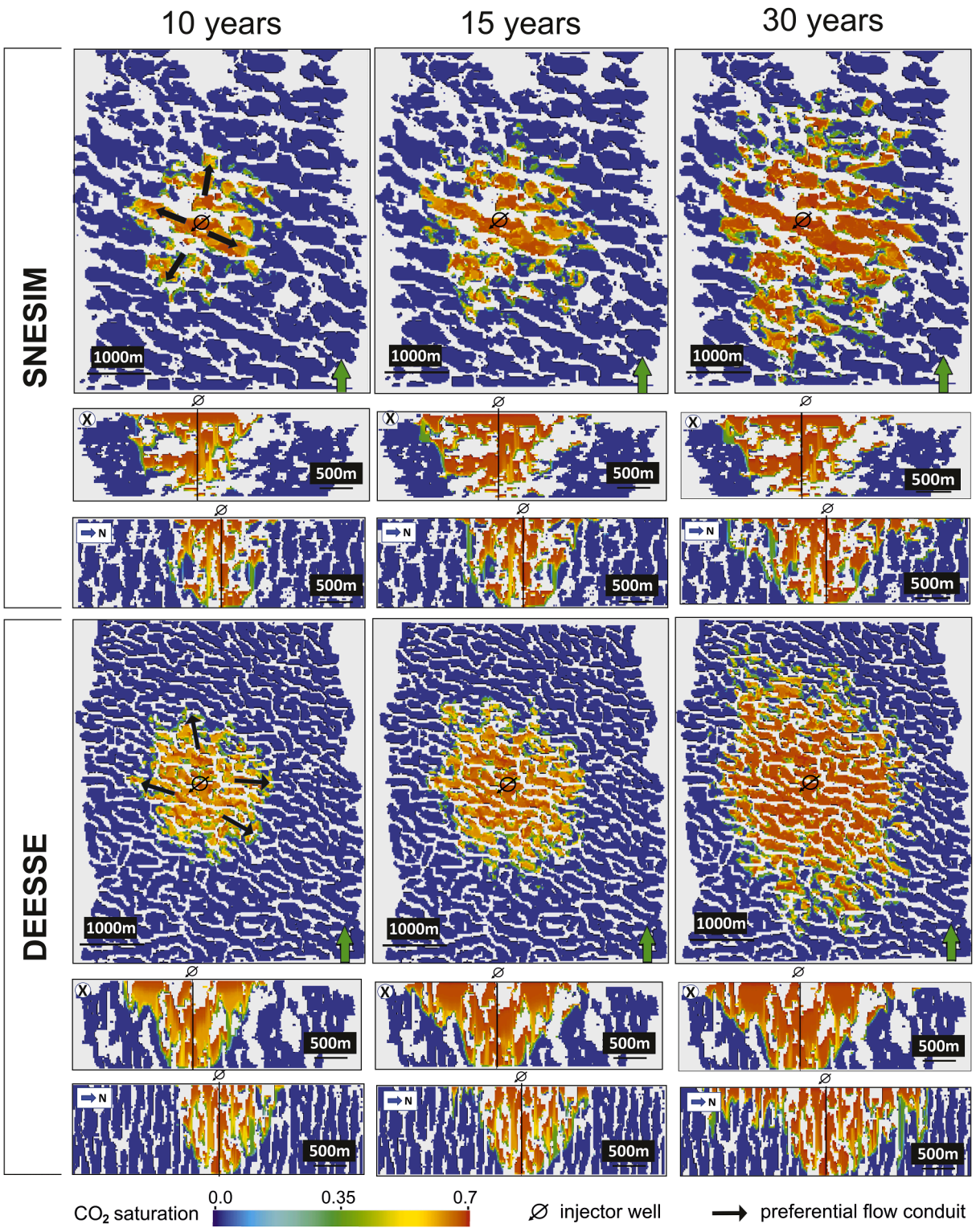

Fig. 8. Plume evolution on horizontal and vertical sections for macroscale-only facies models produced with SNESIM and DEESSE, for ten, fifteen and thirty years of injection. The blue colour indicates brine-saturated volumes. Barriers to flow are represented in white. Horizontal sections are extracted at $Z = 11$ (out of 50 slices). Black arrows indicate the general elongation of preferential flow paths along which the plume tends to propagate. Vertical exaggeration set to a factor of 25.

changes in relative permeabilities.

Dynamic simulations of facies models with mesoscale features created with SNESIM and DEESSE and associated with injection at INJ-1 exhibit similar storage capacities (Fig. 13A). Instead, injection rates during the initial phase of injection differ significantly for the SNESIM and DEESSE grids. Unlike the simulation run on the DEESSE grid, which demonstrates a drop in injection rate in the first few months similar to the one described above for the facies model with macroscale focus, the simulation of the SNESIM grid is characterized by a less rapid but continuous increase in injection rate. The injection rate for the SNESIM grid overtakes the rate for the DEESSE grid in year 3, after which the rate increases relatively steadily in the simulations of both models.

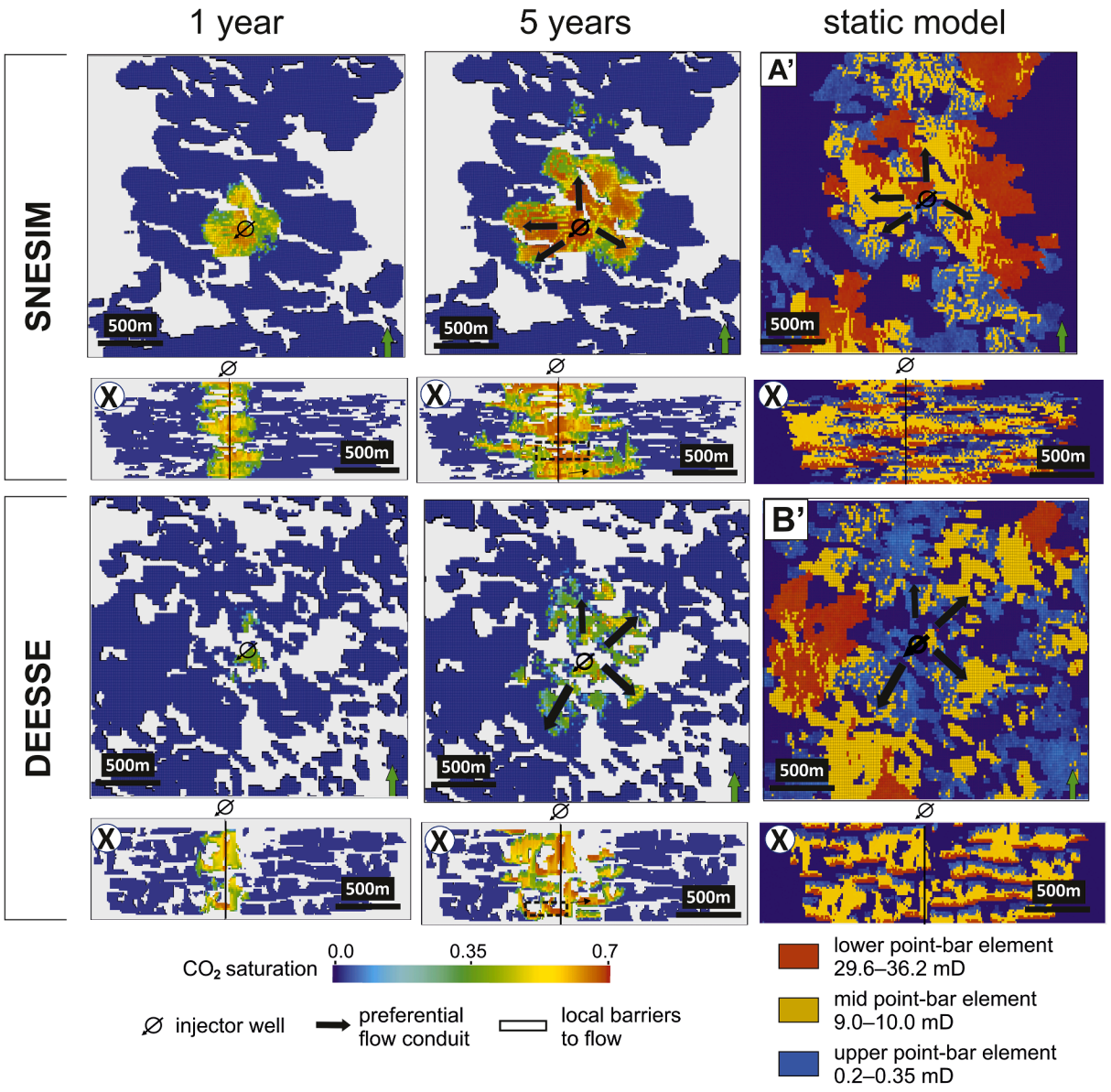

Fig. 9. Plume evolution on horizontal and vertical sections for facies models encompassing mesoscale heterogeneities, produced with SNESIM and DEESSE, for one and five years of injection. Horizontal sections are extracted at $Z = 2$ (out of 50 slices). Black dashed frames highlight CO_2 accumulation under intraformational barriers. Black arrows indicate the general elongation of preferential flow paths along which the plume tends to propagate. On the right, corresponding sections of the static facies models are shown. Vertical exaggeration set to a factor of 25.

Variations in injections rates reflect the impact of the higher sand-body connectivity of the SNESIM mesoscale facies model compared to the DEESSE one, and the absence of significant flow barriers near the area of influence of the well. The differences in architecture across the SNESIM and DEESSE mesoscale models might have resulted in different times at which high CO_2 saturation was reached in the reservoir brine. In both cases, a decrease in injection rates is observed in the last years of injection, even though this is more prominent in the simulation run on the SNESIM grid (Fig. 13B). The decrease in injection rates is due to pressurization of the entire reservoir (Fig. 11), and so an artefact related to the size of the total volume being defined in the dynamic model.

The inclusion of mesoscale heterogeneities has a larger impact on dynamic behaviour compared to the MPS modelling method or the injector location (Fig. 14).

Larger CO_2 cumulative injected volumes and injection rates are seen for facies models including mesoscale heterogeneities, created with both SNESIM and DEESSE. This reflects how the corresponding static models are characterized by different average values of porosity and permeability, which tend to be larger on average for models with mesoscale focus. Vertical profiles of petrophysical properties for the injector well display differences in reservoir quality across the four considered grids; yet these variations do not appear to have exerted a major control on injection rate or storage capacity. The injector wells are in communication with sand-prone deposits over more than 75% of their profile for all models.

4. Discussion

In the planning of CCS projects, the suitability for CO_2 sequestration of highly heterogeneous successions, such as those produced by meandering fluvial systems, has been widely debated (Issautier et al., 2014; Cabello et al., 2018; Sun et al., 2021, 2022, 2023). It is therefore especially important to understand the likely CO_2 plume displacement, injection rates and storage capacity that may be expected for heterogeneous sedimentary successions like those of meander-belt origin (Sun et al., 2021, 2022, 2023; Norouzi et al., 2022).

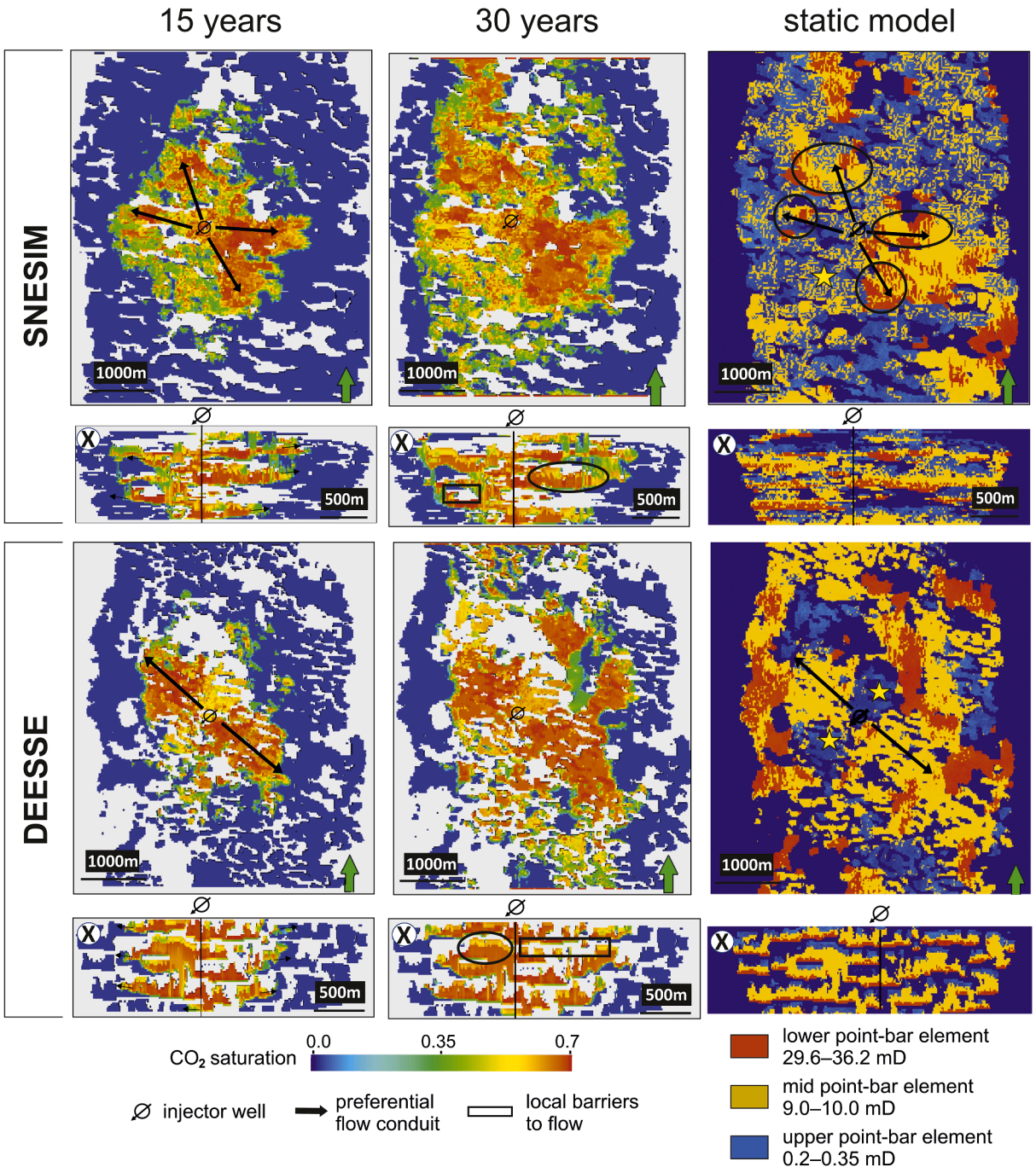

Fig. 10. Plume evolution on horizontal and vertical sections for facies models encompassing mesoscale heterogeneities, produced with SNESIM and DEESSE, for fifteen to thirty years of injection. On the right, corresponding sections of the static facies models are shown. Horizontal sections are extracted at $Z = 12$ (out of 50 slices). Black arrows indicate the general elongation of preferential flow paths along which the plume tends to propagate. The rectangular frames indicate intra-formational barriers to flow. The oval frames highlight sections where the point-bar fining-upward trend affects CO_2 saturation. Yellow stars indicate flow baffles determined by point-bar top facies. Vertical exaggeration set to a factor of 25.

Differences in the outputs of the simulations presented here reveal the impact of different scales of sedimentary heterogeneity on the displacement of a CO_2 plume. Facies models that only consider macro-scale heterogeneity incorporate point-bar sandbodies that are compartmentalized by mud-prone channel-fill and floodplain deposits (Pickup et al., 1994; Pranter et al., 2007; Colombera et al., 2017; Willis and Sech, 2019a, 2019b). By contrast, models that consider mesoscale heterogeneities additionally encapsulate the facies organization of point-bar deposits. The use of the latter type of facies models for scopes of dynamic simulation enables consideration of lithological controls on CO_2 fluid flow, which have been shown to be important in terms of forecasted injection history. Even though there exist limitations in our ability to use MPS geostatistical modelling to reproduce the sedimentary architecture of meander-belt successions (Montero et al., 2021), the results presented in this work highlight how the level of detail with which we model the facies heterogeneity of channel-belt deposits has a larger impact on predicted dynamic behaviour compared to the choice of MPS modelling algorithm. This should be taken into account in reservoir modelling work of similar successions.

Additionally, the outcomes of this study permit a comparison

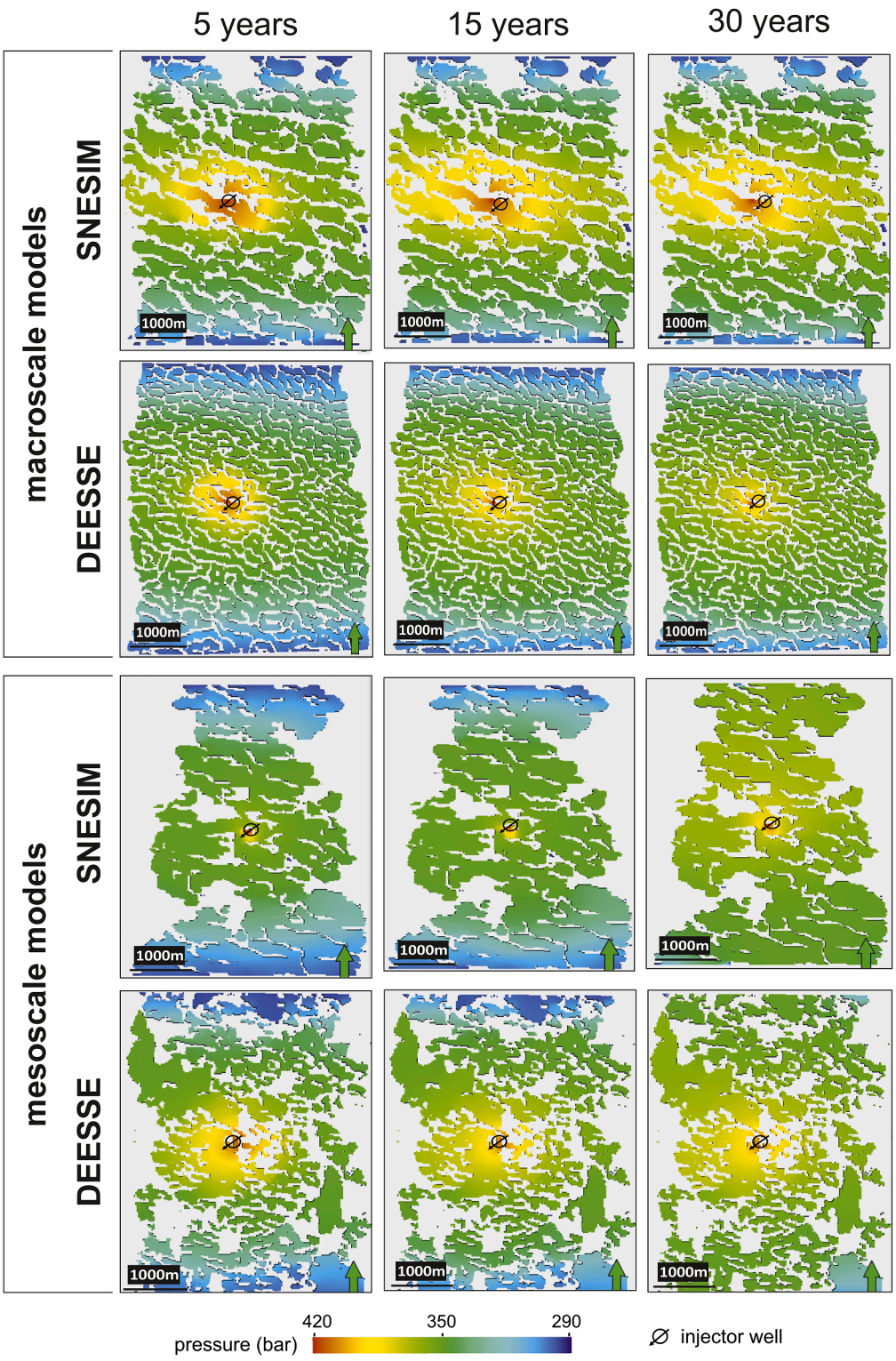

Fig. 11. Pressure distribution over the area of investigation over time (between year 5 and 30) for SNESIM and DEESSE facies models with macro- and meso-scale focus.

between variably heterogeneous meander-belt successions and more homogeneous reservoir types. It has been shown that successions of meandering fluvial systems can provide sufficiently large and interconnected storage capacity, which could make a CCS project economically viable. This is especially the case where individual sand-rich point-bar elements are physically connected with each other. Nonetheless, CO_2 storability will be reduced by point-bar compartmentalization in the presence of mud plugs (channel-fill deposits), whose shape and continuity are in part misrepresented in the MPS models employed here. Furthermore, mud-prone rocks (channel-fill and overbank deposits) may be present in significantly larger fractions, ultimately leading to significantly reduced net volumes. Also, vertical and horizontal heterogeneities that have not been considered here, for example related to the occurrence of fine-grained sediments (e.g., mud drapes) or mud-clast

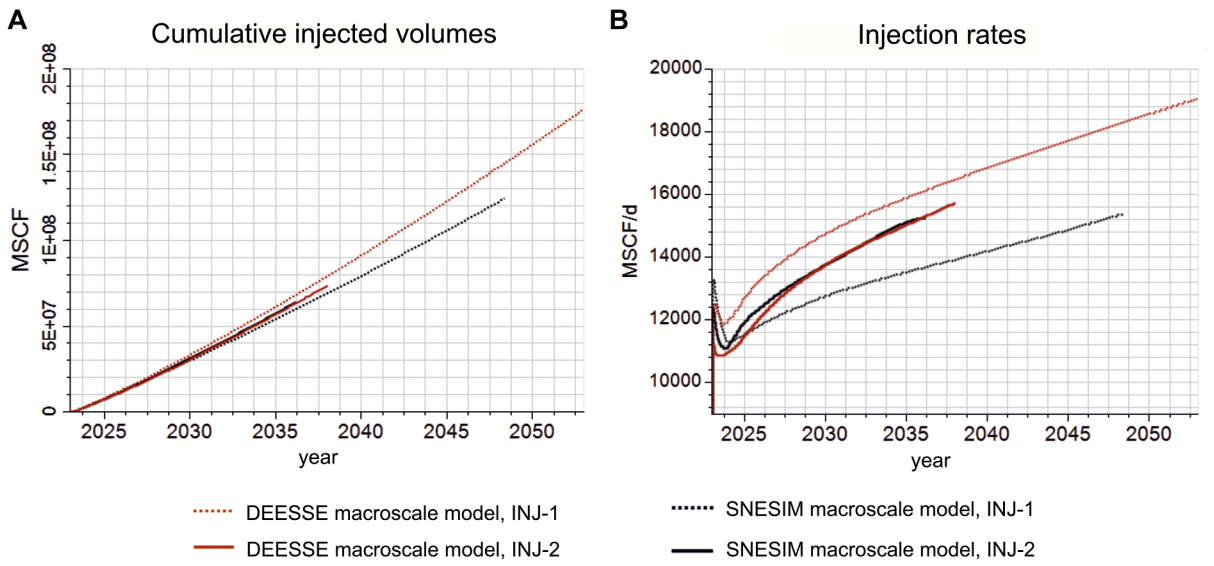

Fig. 12. Plots of (A) cumulative injected volumes (thousand standard cubic feet) and (B) injection rates (thousand standard cubic feet per day) through time for facies models including macroscale heterogeneities only.

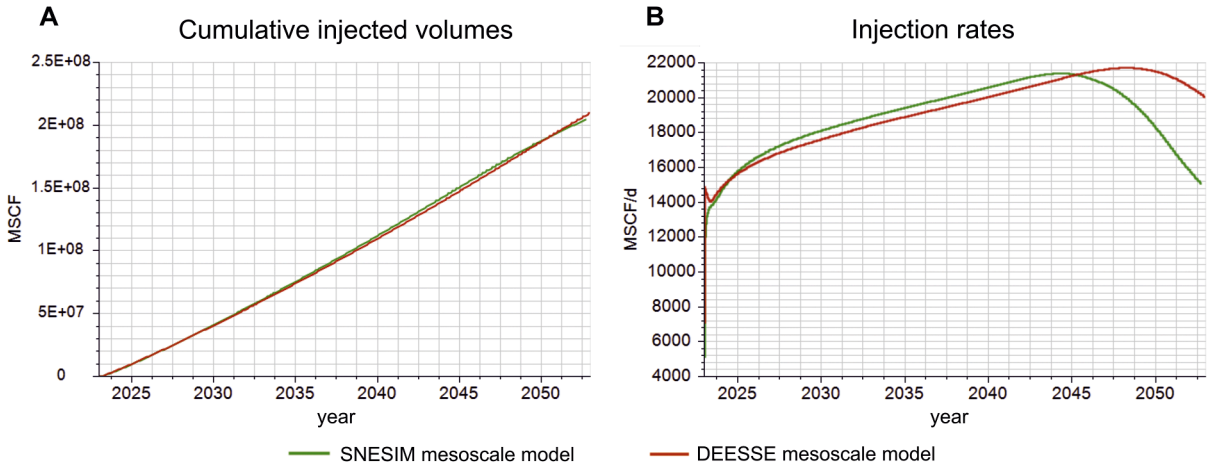

Fig. 13. Plots of (A) cumulative injected volumes (thousand standard cubic feet) and (B) injection rates (thousand standard cubic feet per day) for facies models that incorporate mesoscale features.

conglomerates within the sandbodies, will significantly affect reservoir properties and flow behaviour (Tyler and Finley, 1991; Miall, 1996; Corbett et al., 2012).

Although heterogeneous successions of meandering fluvial systems may be limited in terms of storage capacity and injectivity, compared to more homogeneous successions, there are aspects revealed by this study that may render them well suited in terms of safety and efficiency of CO_2 storage. With regards to valley-fill successions made of vertically stacked channel belts, such as those considered in this study, relatively low-permeability point-bar top units may act as intraformational seals that can help dissipate pressures horizontally, thereby reducing the pressure exerted over the caprock, helping maintain topseal integrity. This effect may also be facilitated by trapping caused by capillary differences between rock types, which may further extend the CO_2 plume horizontally. Additionally, this will result in more limited chemical reactions between the caprock and the CO_2 plume, which may otherwise facilitate leakage. The presence of mud-prone bar-top units may also enable density-driven convective mixing of the brine to take place at different levels through the storage reservoir; compared to an architecturally simpler reservoir, this condition might accelerate CO_2 dissolution (Emami-Meybodi et al., 2015). Also, the tortuosity of flow paths caused by the occurrence of mud-prone rocks will increase the surface area of the plume and therefore the exchange surface between the plume and the reservoir brine, as well as the contact surface with the host rock; this will in turn increase (i) the chance of CO_2 dissolution, ensuring the permanent storage of CO_2 within the reservoir rock; (ii) the likelihood of trapping via mineralization, which may take place thousands of years after injection (Zhang and DePaolo, 2017). However, sand-body tortuosity is also a factor that tends to slow down the rate of spread of the plume and hinder the development of initial flow pathways. This is an especially important element to consider in the characterization of saline aquifers targeted for CCS, for which the likely dynamic behaviour and sealing capacity are particularly uncertain and yet unquantified.

Several aspects of this study may be refined in future work. The very narrow ranges of porosity and permeability values considered in macroscale models allow examination of the influence of larger-scale architectures, but are generally unrealistic. Future studies of this type should additionally aim to incorporate capillary effects, which were disregarded in the current research, but which are crucial to the post-injection evolution of the injected plume (Krevor et al., 2015). There is also scope for improved consideration of relative permeability relationships, which have been shown to control rates of overall plume

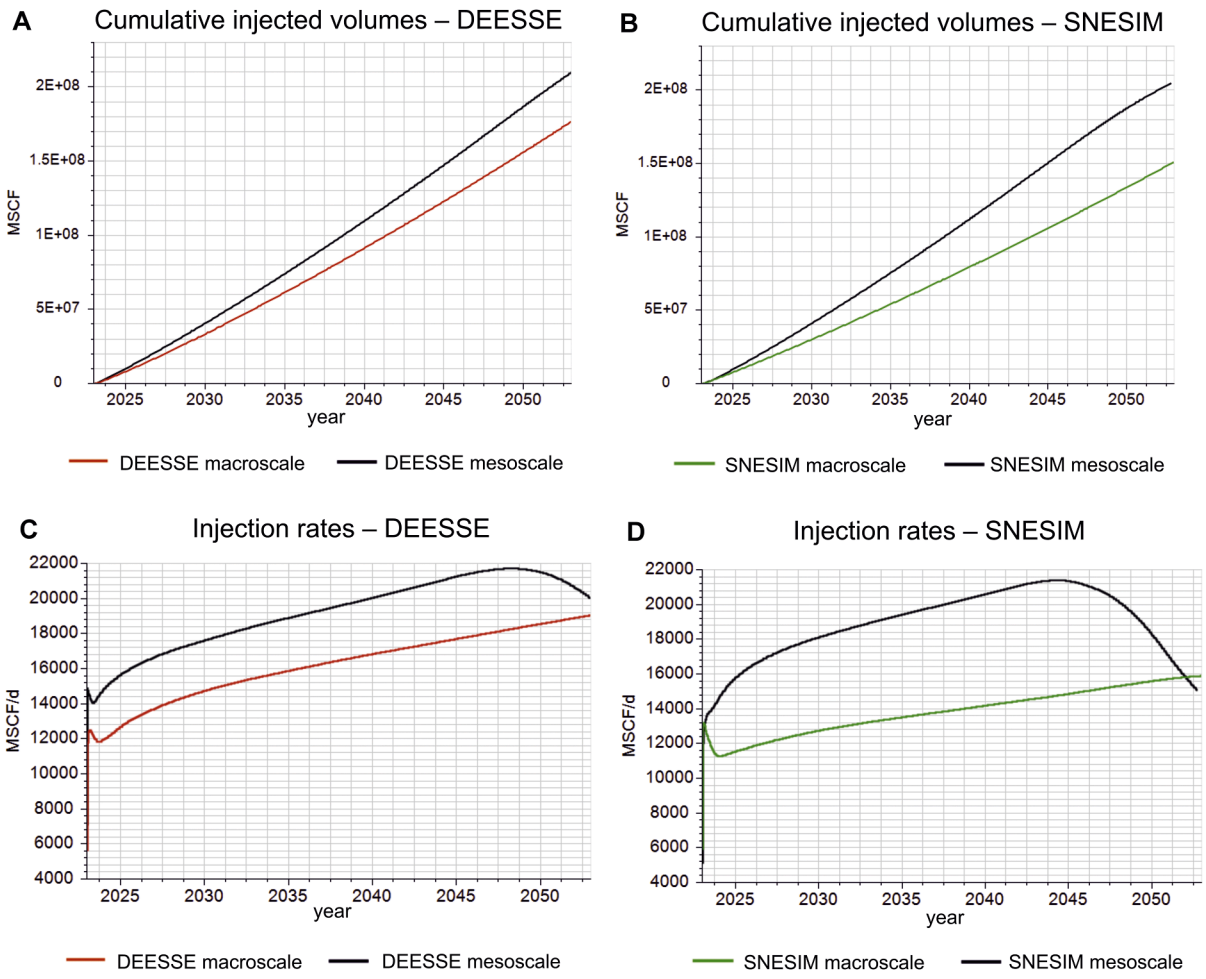

Fig. 14. Cumulative injected volumes (A, B) and injection rates (C, D) for dynamic simulations run on DEESSE and SNESIM grids for macro- and mesoscale heterogeneities.

spread. This could be done by: (i) considering alternatives to the Corey's relative permeability relationships used in this study, such as the Van Genuchten function (Van Genuchten, 1980); (ii) employing bespoke relative-permeability functions for specific lithological categories (cf. Dana et al., 2002; Krevor et al., 2012). Also, the potential impact of permeability anisotropy and microscale (bed-, lamina- and grain-scale; cf. Li and Benson, 2015) heterogeneity in porosity and permeability has been ignored in this research. In particular, the effects of mud drapes mantling bar fronts and of the presence of heterolithic packages deserve further consideration given their widespread occurrence in meander-belt deposits and their impact on static connectivity and petrophysical properties (cf. Thomas et al., 1987; Colombera et al., 2018; Yan et al., 2019). The possible role of diagenesis or fractures on petrophysics could also be considered in future studies.

5. Conclusions

This study elucidates the importance of sedimentary heterogeneities at different scales and of their representation in static models by application of geomodelling tools on the dynamic flow behaviour of a programme of CO_2 injection, with specific focus on successions of meandering fluvial systems. Sedimentary architectures representative of a fluvial valley fill composed of amalgamated meander-belt deposits have been modelled using two MPS geostatistical modelling algorithms: SNESIM and DEESSE. Facies models were produced that consider two alternative levels of detail in the representation of meander-belt facies architecture: (i) macroscale architectural elements only (point-bar and channel-fill elements); and (ii) both macroscale architectures and mesoscale lithological variations within point-bar elements. Static models of porosity and permeability based on geological analogues and constrained on these facies models were employed in dynamic simulations of CO_2 injection over 30 years to investigate the impact of scales of heterogeneities and modelling method on the behaviour of an injected CO_2 plume.

The study reaches the following conclusions:

- Geological heterogeneities in the successions of meandering fluvial systems control the behaviour of injected CO_2 plumes, in terms of trapping efficiency, injection rates and ultimately storage capacity. Higher permeability lower-bar facies act as preferential CO_2 pathways (thief zones), whereas point-bar top facies may act as baffles that retard CO_2 flow. The geometry of mud-prone channel-fill and floodplain deposits control plume tortuosity, which determines the plume surface area, thus impacting dissolution in the brine. Intraformational barriers or baffles related to abandoned channel fills, floodplain deposits and relatively low-permeability point-bar top deposits affect local CO_2 saturation and pressures, reducing the pressure exerted directly on the caprock and CO_2 concentration in its vicinity; this has implications regarding seal integrity. Thus, the choice of resolution at which static models are built should consider the expected impact of architectural features at different scales.
- Plume behaviour and trapping are mainly controlled by petrophysical heterogeneity reflecting the underlying sedimentary framework. Reservoir pressure dominates the behaviour of early injection stages

before a separate CO_2 phase emerges. Permeability contrasts become more important in simulations that consider mesoscale heterogeneities in point-bar elements, which affect the spatial variability in CO_2 saturation content.

- In the type of sedimentary succession modelled here, injection rates are seen to vary through time in relation to temporal variations in the relative importance of: (i) bottom-hole pressure, (ii) CO_2 dissolution in brine, and (iii) emergence of a separate CO_2 phase. The importance and timing of these factors vary in relation to the reservoir connectivity near the well.
- The particular type of facies-modelling approach selected when modelling reservoirs targeted for CCS has a considerable impact on predicted CO_2 plume behaviour. This is true even for different modelling algorithms that are based on the same general principles (multipoint statistics) and are constrained using the same geological inputs (identical training images).

This investigation demonstrates that, compared to more homogeneous reservoir types, successions of meandering fluvial systems may be preferable if architectural characteristics are present that may enhance CO_2 trapping and facilitate pressure management. However, this study also demonstrates that decision making should be supported by a sound reservoir modelling effort that accounts for different forms of heterogeneities.

CRediT authorship contribution statement

Jose M. Montero: Writing – original draft, Methodology, Investigation, Formal analysis, Data curation, Conceptualization. **Luca Colombera:** Writing – review & editing, Supervision, Methodology, Funding acquisition, Formal analysis, Conceptualization. **Enrique Yuste:** Writing – review & editing, Methodology, Investigation, Formal analysis. **Na Yan:** Writing – review & editing, Supervision, Software, Methodology. **Nigel P. Mountney:** Writing – review & editing, Supervision, Methodology, Funding acquisition, Conceptualization.

Declaration of competing interest

The authors declare that they have no known competing financial interests or personal relationships that could have appeared to influence the work reported in this paper.

Data availability

Data will be made available on request.

Acknowledgements

We thank AkerBP, Areva (now Orano), BHPBilliton, Cairn India (Vedanta), ConocoPhillips, Chevron, CNOOC, Equinor, Murphy Oil, Occidental, Saudi Aramco, Shell, Tullow Oil, Woodside and YPF for their financial support of the Fluvial & Eolian Research Group at the University of Leeds. We also thank our project partner Petrotechnical Data Systems for their support. We would also like to thank Philippe Renard and Julien Straubhaar (University of Neuchatel) for providing an academic license to DEESSE. We also thank Schlumberger for providing academic licenses to Petrel and Eclipse. We thank two anonymous reviewers for their constructive comments.

Supplementary materials

Supplementary material associated with this article can be found, in the online version, at doi:10.1016/j.ijggc.2024.104199.

References

Al-Khdheeawi, E.A., Vialle, S., Barifcani, A., Sarmadivaleh, M., Iglauer, S., 2017. Impact of reservoir wettability and heterogeneity on CO2-plume migration and trapping capacity. J. Greenh. Gas Control 58, 142–158. https://doi.org/10.1016/j.ijggc.2017.01.012.

Ambrose, W.A., Lakshminarasimhan, S., Holtz, M.H., Núnez-Lopez, V., Hovorka, S.D., Duncan, I., 2008. Geologic factors controlling CO_2 storage capacity and permanence: case studies based on experience with heterogeneity in oil and gas reservoirs applied to CO2 storage. Environ. Geol. 54 (8), 1619–1633. https://doi.org/10.1007/s00254-007-0940-2.

Bachu, S., Bonijoly, D., Bradshaw, J., Burruss, R., Holloway, S., Christensen, N.P., Mathiassen, O.M., 2007. CO_2 storage capacity estimation: methodology and gaps. Int. J. Greenh. Gas Control 1 (4), 430–443. https://doi.org/10.1016/S1750-5836(07)00086-2.

Bär, K., Reinsch, T., Bott, J., 2020. P^3–PetroPhysical property database–a global compilation of lab measured rock properties. Earth Syst. Sci. Data 12 (4), 2485–2515. https://doi.org/10.5194/essd-12-2485-2020.

Bennion, D.B., Bachu, S., 2006. Dependence on temperature, pressure, and salinity of the IFT and relative permeability displacement characteristics of CO2 injected in deep saline aquifers. In: SPE Annual Technical Conference and Exhibition. San Antonio, Texas, USA. https://doi.org/10.2118/102138-MS. SPE-102138-MS.

Bennion, B., Bachu, S., 2008. Drainage and imbibition relative permeability relationships for supercritical CO_2/brine and H_2S/brine systems in intergranular sandstone, carbonate, shale and anhydrite rocks. SPE Reserv. Eval. Eng. 11, 487–496. https://doi.org/10.2118/99326-PA.

Brandsæter, I., Ringrose, P.S., Townsend, C.T., Omdal, S., 2001. Integrated modeling of geological heterogeneity and fluid displacement: smørbukk gas-condensate field, offshore Mid-Norway. In: Proceedings of the SPE Reservoir Simulation Symposium. Houston, Texas. https://doi.org/10.2118/66391-MS. February 2001.

Bridge, J.S., 2003. Rivers and Floodplains. Forms, Processes, and Sedimentary Record. Blackwell, Oxford, p. 491. https://doi.org/10.1002/jqs.856.

Budinis, S., Krevor, S., Dowell, N.M., Brandon, N., Hawkes, A., 2018. An assessment of CCS costs, barriers and potential. Energy Strategy Rev. 22, 61–81. https://doi.org/10.1016/j.esr.2018.08.003.

Bunch, M.A., Backe, G., Kaldi, J., 2011. Geological appraisal of an onshore CO_2 storage prospect. Energy Procedia 4, 4625–4632. https://doi.org/10.1016/j.egypro.2011.02.422.

Cabello, P., Dominguez, D., Murillo-López, M., López-Blanco, M., Garcia-Sellés, D., Cuevas, J., Marzo, M., Arbués, P., 2018. From conventional outcrop datasets and digital outcrop models to flow simulation in the Pont de Montanyana point-bar deposits (Ypresian, Southern Pyrenees). Mar. Pet. Geol. 94, 19–42. https://doi.org/10.1016/j.marpetgeo.2018.03.040.

Caers, J., Zhang, T., 2004. Multiple-Point Geostatistics: A Quantitative Vehicle for Integration Geologic Analogs Into Multiple Reservoir Model, Integration of Outcrop and Modern Analog Data in Reservoir Models. Stanford University, Stanford Centre for Reservoir Forecasting, Stanford, CA, p. 94305. -2220.

Clark, A.B.S., Thomas, B.M., 1988. The intra-latrobe play: a case history from the Basker/Manta block (VIC/P19), Gippsland basin. APEA J. 28, 100–112.

Colombera, L., Mountney, N.P., McCaffrey, W.D., 2012a. A relational database for the digitization of fluvial architecture concepts and example applications. Pet. Geosci. 18 (1), 129. https://doi.org/10.1144/1354-079311-021.

Colombera, L., Felletti, F., Mountney, N.P., McCaffrey, W.D., 2012b. A database approach for constraining stochastic simulations of the sedimentary heterogeneity of fluvial reservoirs. Am. Assoc. Pet. Geol. Bull. 96 (11), 2143–2166. https://doi.org/10.1306/04211211179.

Colombera, L., Mountney, N.P., McCaffrey, W.D., 2013. A quantitative approach to fluvial facies models: methods and example results. Sedimentology 60 (6), 1526–1558. https://doi.org/10.1111/sed.12050.

Colombera, L., Mountney, N.P., Russell, C.E., Shiers, M.N., McCaffrey, W.D., 2017. Geometry and compartmentalization of fluvial meander-belt reservoirs at the bar-form scale: quantitative insight from outcrop, modern and subsurface analogues. Mar. Pet. Geol. 82, 35–55. https://doi.org/10.1016/j.marpetgeo.2017.01.024.

Colombera, L., Yan, N., McCormick-Cox, T., Mountney, N.P., 2018. Seismic-driven geocellular modeling of fluvial meander-belt reservoirs using a rule-based method. Mar. Pet. Geol. 93, 553–569. https://doi.org/10.1016/j.marpetgeo.2018.03.042.

Corbett, P., Hamdi, H., Gurav, H., 2012. Layered fluvial reservoirs with internal fluid cross flow: a well-connected family of well test pressure transient response. Pet. Geosci. 18 (2), 219–229. https://doi.org/10.1144/1354-079311-008.

Corey, A.T., 1954. The interrelation between gas and oil relative permeabilities. Prod. Mon. 19, 38–41.

Dai, Z., Zhang, S., Wang, Y., Li, X., Cao, H., 2014. Short-term safety risk assessment of CO2 geological storage projects in deep saline aquifers using the Shenhua CCS Demonstration Project as a case study. Environ. Earth Sci. 73, 7571–7586. https://doi.org/10.1007/s12665-014-3928-8.

Dana, E., Skoczylas, F., 2002. Experimental study of two-phase flow in three sandstones. I. Measuring relative permeabilities during two-phase steady-state experiments. Int. J. Multiph. Flow 28 (11), 1719–1736. https://doi.org/10.1016/S0301-9322(02)00090-3.

Eiken, O., Ringrose, P., Hermanrud, C., Nazarian, B., Torp, T.A., Hoier, L., 2011. Lessons learned from 14 years of CCS operations: sleipner, In Salah and Snøhvit. Energy Procedia 4, 5541–5548. https://doi.org/10.1098/rsfs.2019.0065.

Emami-Meybodi, H., Hassanzadeh, H., Green, C.P., Ennis-King, J., 2015. Convective dissolution of CO2 in saline aquifers: progress in modeling and experiments. J. Greenh. Gas Control 40, 238–266. https://doi.org/10.1016/j.ijggc.2015.04.003.

Espinoza, D.N., Santamarina, J.C., 2017. CO_2 breakthrough-caprock sealing efficiency and integrity for carbon geological storage. J. Greenh. Gas Control l (66), 218–229. https://doi.org/10.1016/j.ijggc.2017.09.019.

Flett, M., Gurton, R., Weir, G., 2007. Heterogeneous saline formations for carbon dioxide disposal: impact of varying heterogeneity on containment and trapping. J. Pet. Sci. Eng. 57 (1–2), 106–118. https://doi.org/10.1016/j.petrol.2006.08.016.

Friend, P.F., 1983. Towards the field classification of alluvial architecture or sequence. In: Modern and Ancient Fluvial Systems, 6. International Association of Sedimentologists, Special Publication, pp. 345–354. https://doi.org/10.1002/9781444303773.ch28 (eds Collinson J.D., Lewin J.).

Ghazi, S., Mountney, N.P., 2009. Facies and architectural element analysis of a meandering fluvial succession: the Permian Warchha Sandstone, Salt Range, Pakistan. Sediment. Geol. 221 (1–4), 99–126. https://doi.org/10.1016/j.sedgeo.2009.08.002.

Gershenzon, N., Ritzi, R., Dominic, D., Mehnert, E., 2017. Effective constitutive relations for simulating CO_2 capillary trapping in heterogeneous reservoirs with fluvial sedimentary architecture. Geomech. Geophys. Geo-Energy Ge-Resour. 3 https://doi.org/10.1007/s40948-017-0057-3.

Gibling, M., 2006. Width and thickness of fluvial channel bodies and valley fills in the geological record: a literature compilation and classification. J. Sediment. Res. 76 (5), 731–770. https://doi.org/10.2110/jsr.2006.060.

Glenton, P.N., Sutton, J.T., McPherson, J.G., Fittall, M.E., Moore, M.A., Heavysege, R.G., Box, D., 2013. Hierarchical approach to facies and property distribution in a basin-floor fan model, Scarborough Gas Field, Northwest Shelf, Australia. In: Proceedings of the 6th International Petroleum Technology Conference. Beijing, China.

Global CCS Institute, 2020. Global Statistics of CCS. https://www.globalccsinstitute.com/wp-content/uploads/2021/03/Global-Status-of-CCS-Report-English.pdf.

Guardiano, F.B., Srivastava, R.M., 1993. Multivariate geostatistics: beyond bivariate moments. In: Soares, A. (ed). In: Geostatistics Tróia '92. Quantitative Geology and Geostatistics, 5. Springer, pp. 133–144. https://doi.org/10.1007/978-94-011-1739-5_12.

Haghbakhsh, R., Soleymani, H., Raeissi, S., 2013. A simple correlation to predict high pressure solubility of carbon dioxide in 27 commonly used ionic liquids. J. Supercrit. Fluids 77, 158–166. https://doi.org/10.1016/j.supflu.2013.02.022.

Haldorsen, H.H., MacDonald, C.J., 1987. Stochastic modelling of underground reservoir facies. SPE paper presented at the. In: Proceedings of the SPE Annual Technical Conference and Exhibition. Dallas, Texas. https://doi.org/10.2118/16751-MS. SPE-16751-MS.

Hickin, E.J., 1993. Fluvial facies models: a review of Canadian research. Prog. Phys. Geogr. Earth Environ. 17 (2), 205–222. https://doi.org/10.1177/030913339301700020.

Holden, L., Hauge, R., Skare, Ø., Skorstad, A., 1998. Modeling of fluvial reservoirs with object models. Math. Geol. 30 (5), 473–496. https://link.springer.com/article/10.1023/A:1021769526425.

Iglauer, S., 2018. Optimum storage depths for structural CO_2 trapping. Int. J. Greenh. Gas Control 77, 82–87. https://doi.org/10.1016/j.ijggc.2018.07.009.

Issautier, B., Fillacier, S., Le Gallo, Y., Audigane, P., Chiaberge, C., Viseur, S., 2013. Modelling of CO_2 injection in fluvial sedimentary heterogeneous reservoirs to assess the impact of geological heterogeneities on CO_2 storage capacity and performance. Energy Procedia 37, 5181–5190. https://doi.org/10.1016/j.egypro.2013.06.434.

Issautier, B.S., Viseur, S., Audigane, P., Nindre, Y.M., 2014. Impacts of fluvial reservoir heterogeneity on connectivity: implications in estimating geological storage capacity for CO_2. J. Greenh. Gas Control, 20, 333–349. https://doi.org/10.1016/j.egypro.2013.06.434.

Juanes, R., Spiteri, E.J., Orr, F.M., Blunt, M.J., 2006. Impact of relative permeability hysteresis on geological CO_2 storage. Water Resour. Res. 42 (12) https://doi.org/10.1029/2005WR004806.

Krevor, S.C., Pini, R., Zuo, L., Benson, S.M., 2012. Relative permeability and trapping of CO2 and water in sandstone rocks at reservoir conditions. Water Resour. Res. 48 (2), W02532. https://doi.org/10.1029/2011WR010859.

Krevor, S., Blunt, M.J., Benson, S.M., Pentland, C.H., Reynolds, C., Al-Menhali, A., Niu, B., 2015. Capillary trapping for geologic carbon dioxide storage–From pore scale physics to field scale implications. J. Greenh. Gas Control 40, 221–237. https://doi.org/10.1016/j.ijggc.2015.04.006.

Langford, R., 2016. Carbon Dioxide Potential of the Gippsland Basin: Results of a Study Undertaken As Part of the National CO2 Infrastructure Plan. Geoscience Australia, Canberra. https://doi.org/10.11636/Record.2016.032. Record 2016/32.

Larue, D., Hovadik, J., 2006. Connectivity of channelized reservoirs: a modelling approach. Pet. Geosci. 12 (4), 291–308. https://doi.org/10.1144/1354-079306-699.

Li, B., Benson, S.M., 2015. Influence of small-scale heterogeneity on upward CO2 plume migration in storage aquifers. Adv. Water Resour. 83, 389–404. https://doi.org/10.1016/j.advwatres.2015.07.010.

Liu, Y., Harding, A., Gilbert, R., Journel, A.G., 2004. A workflow for multiple-point geostatistical simulation. In: Leuangthong O., Deutsch C.V. (eds). In: Geostatistics Banff 2004. Quantitative Geology and Geostatistics, 14. Springer, pp. 245–254. https://doi.org/10.1007/978-1-4020-3610-1_25.

Lunt, I.A., Bridge, J.S., Tye, R.S., 2004. A quantitative, three-dimensional depositional model of gravelly braided rivers. Sedimentology 51, 377–414. https://doi.org/10.1111/j.1365-3091.2004.00627.x.

Mariethoz, G., Renard, P., Straubhaar, J., 2010. The Direct Sampling method to perform multiple point geostatistical simulations. Water Resour. Res. 46 (11), 1–14. https://doi.org/10.1029/2008WR007621.

Miall, A.D., 1985. Architectural-element analysis: a new method of facies analysis applied to fluvial deposits. Earth Sci. Rev. 22 (4), 261–308. https://doi.org/10.1016/0012-8252(85)90001-7.

Miall, A.D., 1988. Architectural elements and bounding surfaces in fluvial deposits: anatomy of the Kayenta Formation (Lower Jurassic), southwest Colorado. Sediment. Geol. 55 (3–4), 233–262. https://doi.org/10.1016/0037-0738(88)90133-9.

Miall, A.D., 1996. The Geology of Fluvial Deposits. Sedimentary Facies, Basin Analysis and Petroleum Geology. Springer, p. 582. https://doi.org/10.1007/978-3-662-03237-4.

Miall, A.D., 2016. Stratigraphy: A Modern Synthesis. Springer, p. 454. https://doi.org/10.1007/978-3-319-24304-7.

Moodie, N., Pan, F., Jia, W., McPherson, B., 2016. Impacts of relative permeability formulation on forecasts of CO2 phase behavior, phase distribution, and trapping mechanisms in a geologic carbon storage reservoir. Greenh. Gases Sci. Technol. 7, 241–258. https://doi.org/10.1002/ghg.1610v.

Moore, P.S., Burns, B.J., Emmett, J.K., Guthrie, D.A., 1992. Integrated source, maturation and migration analysis, Gippsland Basin, Australia. APPEA J. 32 (1), 313–324.

Montero, J.M., Colombera, L., Yan, N., Mountney, N.P., 2021. A workflow for modelling fluvial meander-belt successions: combining forward stratigraphic modelling and multi-point geostatistics. J. Pet. Sci. Eng. 201, 108411 https://doi.org/10.1016/j.petrol.2021.108411.

Nalley, S., LaRose, A., 2021. Annual Energy Outlook 2021. Energy Information Administration, Washington, DC, USA.

Nguyen, M., Zhang, X., Ning, W., Jun, L., Xiaochun, L., Zhang, Y., Philip, S., 2017. An object-based modeling and sensitivity analysis study in support of CO_2 storage in deep saline aquifers at the Shenhua site, Ordos Basin. Geomech. Geophys. Geo-Energy Geo-Resour. 3, 293–314. https://doi.org/10.1016/j.esr.2018.08.003.

Norouzi, A., Gluyas, J., Babaei, M., 2022. CO_2-plume geothermal in fluvial formations: a 2D numerical performance study using subsurface metrics and upscaling. Geothermics 99 (4), 40–54. https://doi.org/10.1016/j.geothermics.2021.102287.

North, C.P., 1996. The prediction and modelling of subsurface fluvial stratigraphy. In: Carling, P.A., Dawson, M.R. (Eds.), Advances in Fluvial Dynamics and Stratigraphy. John Wiley & Sons, Chichester, pp. 395–508.

Pickup, G.E., Ringrose, P.S., Forrester, M.M., Jensen, J.L., Sorbie, K.S., 1994. The Geopseudo Atlas: geologically based upscaling of multiphase flow. In: Proceedings of the European Petroleum Computer Conference. Aberdeen, UK, pp. 277–289. https://doi.org/10.2118/27565-MS. SPE 27565.

Petroconsultants, 1996. Petroleum Exploration and Production Database. Petroconsultants Inc., Houston [database available from Petroconsultants, Inc., P.O. Box 740619TX 77274-0619].

Pranter, M.J., Hewlett, A.C., Cole, R.D., Wang, H., Gilman, J., 2013. Fluvial architecture and connectivity of the Williams Fork Formation: use of outcrop analogues for stratigraphic characterization and reservoir modelling. In: Martinius, A.W., Howell, J.A., Good, T.R. (Eds.), Sediment-Body Geometry and Heterogeneity: Analogue Studies for Modelling the Subsurface, 387. Special Publications, Geological Society, London, pp. 57–83. doi:10.1144/SP387.1.

Puig, J.M., Cabello, P., Howell, J., Arbués, P., 2019. Three-dimensional characterisation of sedimentary heterogeneity and its impact on subsurface flow behaviour through the braided-to-meandering fluvial deposits of the Castissent Formation (late Ypresian, Tremp-Graus Basin, Spain). Mar. Pet. Geol. 103, 661–680. https://doi.org/10.1016/j.marpetgeo.2019.02.014.

Pyrcz, M.J., Deutsch, C.V., 2014. Geostatistical Reservoir Modeling. Oxford University Press, USA.

Quinn, M., 2022. Carbon capture and storage: a review of Australian projects. APPEA J. 62 (1), 334–341. https://doi.org/10.1071/AJ21161.

Reading, H.G., 2001. Clastic facies models: a personal perspective. Bull. Geol. Soc. Den. 48, 101–125. http://doi.org/10.37570/bgsd-2001-48-05.

Riaz, A., Cinar, Y., 2014. Carbon dioxide sequestration in saline formations: part I. Review of the modeling of solubility trapping. J. Pet. Sci. Eng. 124, 367–380. https://doi.org/10.1016/j.petrol.2014.07.024.

Ringrose, P., Bentley, M., 2015. Reservoir Model Design: A Practitioner's Guide. Springer Science & Business Media B.V., Berlin, p. 260. https://doi.org/10.1007/978-94-007-5497-3.

Ringrose, P.S., Furre, A.K., Gilfillan, S.M.V., Krevor, S., Landroslash, M., Leslie, R., Meckel, T., Nazarian, B., Zahid, A., 2021. Storage of carbon dioxide in saline aquifers: physicochemical processes, key constraints, and scale-up potential. Annu. Rev. Chem. Biomol. Eng. 12, 471–494. https://doi.org/10.1146/annurev-chembioeng-093020-091447.

Riordan, S.J., Lang, S.C., Payenberg, T., 2004. Sequence stratigraphy of the intra-Latrobe Group, Flounder Field, Gippsland Basin. Implications for the building and upscaling of 3D geological models. In: Proceedings of the PESA Eastern Australasian Basins Symposium, II, pp. 523–536.

Shiers, M.N., Mountney, N.P., Hodgson, D.M., Cobain, S.L., 2014. Depositional controls on tidally influenced fluvial successions, Neslen Formation, Utah, USA. Sediment. Geol. 311, 1–16. https://doi.org/10.1016/j.sedgeo.2014.06.005.

Singh, V.P., Cavanagh, A., Hansen, H., Nazarian, B., Iding, M., Ringrose, P.S., 2010. Reservoir modeling of CO2 plume behaviour calibrated against monitoring data from Sleipner, Norway. SPE paper presented at. In: Proceedings of the SPE Annual Technical Conference and Exhibition. Florence, Italy. https://doi.org/10.2118/134891-MS. SPE-134891-MS.

Soltanian, M.R., Hajirezaie, S., Hosseini, S.A., Dashtian, H., Amooie, M.A., Meyal, A., Ershadnia, R., Ampomah, W., Islam, A., Zhang, X., 2019. Multicomponent reactive transport of carbon dioxide in fluvial heterogeneous aquifers. Nat. Gas Sci. Eng. 65, 212–223. https://doi.org/10.1016/j.jngse.2019.03.011.

Spiteri, E.J., Juanes, R., Blunt, M.J., Orr, F.M., 2005. Relative permeability hysteresis: trapping models and application to geological CO_2 sequestration. SPE paper presented at. In: Proceedings of the SPE Annual Technical Conference and Exhibition. Dallas, Texas. https://doi.org/10.2118/96448-MS. SPE-96448-MS.

Stalker, L., Gent, D.V., NGL Project Team, 2014. South west hub CCS Project in Western Australia–characterization of a Greenfield site. Energy Procedia 63, 5041–5050. https://doi.org/10.1016/j.egypro.2014.11.534.

Strebelle, S., 2002. Conditional simulation of complex geological structures using multiple-point statistics. Math. Geol. 34 (1), 1–21. https://doi.org/10.1023/A:1014009426274.

Sun, X., Alcalde, J., Bakhtbidar, M., Elío, J., Vilarrasa, V., Canal, J., Ballesteros, J., Heinemann, N., Haszeldine, S., Cavanagh, A., Vega-Maza, D., Rubiera, F., Martínez-Orio, R., Johnson, G., Carbonell, R., Marzan, I., Travé, A., Gomez-Rivas, E., 2021. Hubs and clusters approach to unlock the development of carbon capture and storage–case study in Spain. Appl. Energy 300, 117418. https://doi.org/10.1016/j.petrol.2021.108411.

Sun, X., Gomez-Rivas, E., Cruset, D., Alcalde, J., Munoz-Lopez, D., Cantarero, I., Martín-Martín, J.D., John, C.M., Travé, A., 2022. Origin and distribution of calcite cements in a folded fluvial succession: the Puig-reig anticline (south-eastern Pyrenees). Sedimentology 69, 2319–2347. https://doi.org/10.1111/sed.12994. https://onlinelibrary.wiley.com/.

Sun, X., Cao, Y., Liu, K., Alcalde, J., Cabello, P., Travé, A., Cruset, D., Gomez-Rivas, E., 2023. Effects of fluvial sedimentary heterogeneity on CO_2 geological storage: integrating storage capacity, injectivity, distribution and CO_2 phases. J. Hydrol. 617, 128936 https://doi.org/10.1016/j.jhydrol.2022.128936.

Thomas, R.G., Smith, D.G., Wood, J.M., Visser, J., Calverley-Range, E.A., Koster, E.H., 1987. Inclined heterolithic stratification–terminology, description, interpretation and significance. Sediment. Geol. 53 (2), 123–179. https://doi.org/10.1016/S0037-0738(87)80006-4.

Tyler, N., Finley, R.J., 1991. Architectural controls on the recovery of hydrocarbons from sandstone reservoirs. In: Miall, A.D., Tyler, N. (Eds.), The Three-Dimensional Facies Architecture of terrigenous Clastic Sediments and Its Implications for Hydrocarbon Discovery and Recovery. SEPM (Society for Sedimentary Geology), pp. 1–5. Concepts in Sedimentology and Palaeontology 3, Society for Sedimentary Geology. doi:10.2110/csp.91.03.0001.

UK Office for National Statistics, 2022. UK Environmental Accounts: 2022. UK Office for National Statistics Statistical Bulletin.

UNFCCC, 2018. The paris agreement - publication. Paris Climate Change Conference - November 2015. UNFCCC Publications.

Van Genuchten, M.T., 1980. A closed-form equation for predicting the hydraulic conductivity of unsaturated soils. Soil Sci. Soc. Am. J. 44, 892–898. https://doi.org/10.2136/sssaj1980.03615995004400050002x.

Walker, R.G., 1984. General introduction: facies, facies sequences and facies models. In: facies Models. Geological Association of Canada Reprint Series, 2nd ed. Geological Association of Canada, Toronto, pp. 1–9 https://cir.nii.ac.jp/crid/1571135650747572736.

Willis, B.J., Sech, R.P., 2019a. Quantifying impacts of fluvial intra-channel-belt heterogeneity on reservoir behaviour. In: Fluvial Meanders and Their Sedimentary Products in the Rock Record, 48. International Association of Sedimentologists, Special Publication, pp. 543–572. https://doi.org/10.1002/9781119424437.ch20 (eds M. Ghinassi, L. Colombera, N.P. Mountney, A.J.H. Reesink).

Willis, B.J., Sech, R.P., 2019b. Emergent facies patterns within fluvial channel belts. In: Fluvial Meanders and Their Sedimentary Products in the Rock Record, 48. International Association of Sedimentologists, Special Publication, pp. 509–542. https://doi.org/10.1002/9781119424437.ch19 (eds M. Ghinassi, L. Colombera, N. P. Mountney, A.J.H. Reesink).

Yan, N., Mountney, N.P., Colombera, L., Dorrell, R.M., 2017. A 3D forward stratigraphic model of fluvial meander-bend evolution for prediction of point-bar lithofacies architecture. Comput. Geosci. 105 (7), 65–80. https://doi.org/10.1016/j.cageo.2017.04.012.

Yan, N., Colombera, L., Mountney, N.P., Dorrell, D.M., 2019. Three-dimensional modelling of fluvial point-bar architecture and facies heterogeneity using analogue data and associated analysis of intra-bar static connectivity: application to humid coastal-plain and dryland fluvial systems. In: Fluvial Meanders and Their Sedimentary Products in the Rock Record, 48. International Association of Sedimentologists, Special Publication, pp. 475–508. https://doi.org/10.1002/9781119424437.ch18 (eds M. Ghinassi, L. Colombera, N.P. Mountney, A.J.H. Reesink).

Zhang, S., DePaolo, D., 2017. Rates of CO_2 mineralization in geological carbon storage. Acc. Chem. Res. 50. https://10.1021/acs.accounts.7b00334.